Biophysical Journal Volume 65 November 1993 2160–2177

Influence of Surface Chemistry on the Structural Organization of Monomolecular Protein Layers Adsorbed to Functionalized Aqueous Interfaces

Mathias Lösche,* Michael Piepenstock,* Anke Diederich,* Torsten Grünewald,* Kristian Kjaer,‡ and David Vaknin§

*Institute of Physical Chemistry, Johannes-Gutenberg-Universität Mainz, D-55099 Mainz, Germany; ‡Physics Department, Risø National Laboratory, DK-4000 Roskilde, Denmark; and §Ames Laboratory, Physics Department, Iowa State University, Ames, Iowa 50011 USA

ABSTRACT The molecular organization of streptavidin (SA) bound to aqueous surface monolayers of biotin-functionalized lipids and binary lipid mixtures has been investigated with neutron reflectivity and electron and fluorescence microscopy. The substitution of deuterons (^{2}H) for protons (^{1}H), both in subphase water molecules and in the alkyl chains of the lipid surface monolayer, was utilized to determine the interface structure on the molecular length scale. In all cases studied, the protein forms monomolecular layers underneath the interface with thickness values of ~40 Å. A systematic dependence of the structural properties of such self-assembled SA monolayers on the surface chemistry was observed: the lateral protein density depends on the length of the spacer connecting the biotin moiety and its hydrophobic anchor. The hydration of the lipid head groups in the protein-bound state depends on the dipole moment density at the interface.

INTRODUCTION

The control of the structural organization of molecules at surfaces is a key for interface functionalization, and thus for the design of advanced materials (Swalen et al., 1987). Such control, however, requires ultrasensitive characterization techniques, since minute amounts of materials suffice for surface functionalization. A process that gains progressively more importance for interface modification involves the specific binding of proteins at surfaces, utilizing the molecular recognition principle developed in the course of evolution in living cells for a number of purposes, such as immunoresponse, biocatalysis, and communication (Alberts et al., 1983). Immobilized proteins have been utilized in numerous applications in biotechnology (Carr and Bowers, 1980; Gronow, 1991). With the recent advent of novel sensitive techniques capable of characterizing interface structures on the molecular length scale (Möhwald, 1990) it is now possible to optimize such systems on the basis of a molecular comprehension of the interface structure.

The engineering of functionalized solid surfaces on the molecular length scale can be achieved by two routes (Swalen et al., 1987): molecular layers of the functional moiety can either be attached directly to a solid interface by adsorption from solutions (Sagiv, 1980; Ebersole et al., 1990), or they can be formed and manipulated at gas-liquid interfaces and subsequently transferred to solid substrates (Hafeman et al., 1981). From an applied science perspective, the characterization of the resulting solid surface may be of greater immediate importance (Ebersole et al., 1990). However, the ease by which molecular organic layers on liquid surfaces may be manipulated to yield desired structural properties (Egger et al., 1990) makes them attractive systems for the investigation of the underlying organization principles. In addition, the aqueous subphase presents a molecularly smooth interface, with a residual roughness that may be due to thermally excited capillary waves (Als-Nielsen and Kjaer, 1989; Sanyal et al., 1991), and results in samples with better homogeneity than those prepared on most solid supports.

It has been established that protein molecules can be coupled to fluid surfaces in well-defined structures by the functionalization of interfaces (Uzgiris and Kornberg, 1983; Tamm, 1988; Pisarchick and Thompson, 1990). In such experiments, monomolecular lipid surface layers present receptors to the aqueous subphase into which a corresponding protein is dissolved. If the mobility of surface-bound protein parallel to the interface remains large enough, lateral self-organization into two-dimensional (2D) crystals may occur. This was demonstrated by electron diffraction of uranyl stained samples (Ludwig et al., 1986; Reed et al., 1987; Ribi et al., 1987; Darst et al., 1991). The preparation and manipulation of such 2D protein aggregates is of importance in cases where proteins do not readily form 3D crystals (Henderson et al., 1990; Mosser et al., 1991; Mosser and Brisson, 1991).

As a model system for our investigations we used the well-characterized streptavidin-biotin system (Chaiet and Wolf, 1964; Wilchek and Bayer, 1988; Weber et al., 1989). Streptavidin (SA), a tetrameric protein extracted from *Streptomyces avidinii* of ~55 kDa, has an exceptionally high affinity to biotin with a binding constant comparable to that of covalent bonds. It can bind four ligands, two at each of two opposing faces. Recently, we have characterized the structural organization of SA adsorbed to an aqueous surface functionalized with a biotinylated lipid (Vaknin et al., 1991a, 1993; Lösche et al., 1992; Lösche, 1992). On this molecule,

Received for publication 16 June 1993 and in final form 22 July 1993.

Address reprint requests to Dr. Mathias Lösche at the Institute of Physical Chemistry, Johannes-Gutenberg-Universität Mainz, D-55099 Mainz, Germany.

0006-3495/93/11/2160/18 $2.00

the biotin was directly attached to the lipid head group. We have established that the protein organizes in monomolecular layers and have determined the dry volume and the lateral density of the protein by the interpretation of x-ray and neutron reflectivity measurements with space-filling molecular models (Vaknin et al., 1993). In the present study we report the organization of SA bound to biotinylated DPPE, deposited at the interface as the pure compound and in binary mixtures with unfunctionalized lipids. In this system, the biotin is attached to the lipid head group via a caproyl spacer, so that it may be presented to the subphase at a larger distance from the aqueous interface. We thus investigate the question: how does the structural organization of the self-assembled protein monolayer depend on surface chemistry?

MATERIALS AND METHODS

Neutron reflectivity of interfaces

The optics of x-ray and neutron reflectivities of interfaces have been treated in detail in recent reviews (Als-Nielsen and Kjaer, 1989; Russell, 1990). In the experiments reported here, a monochromatic neutron beam with wave vector $\vec{k}_o$, incident at an angle α_o on an aqueous surface, is specularly reflected (i.e., exit angle, $\alpha_r = \alpha_o \equiv \alpha$) with wave vector $\vec{k}_r$ (cf. Fig. 1), and thus the scattering vector, $\vec{Q} = \vec{k}_r - \vec{k}_o$, is strictly parallel to the surface normal, $\vec{z}$. By monitoring the incident and the reflected neutron intensities, I_o and I_r, the reflectivity $R = I_r/I_o$ is reported as a function of $\vec{Q}$. A brief account of the neutron reflectivity of interfaces is given in the Appendix. For a schematic representation of the Fresnel reflectivity, R_F, of a clean fluid interface, refer to Fig. A2 in the Appendix. Reflectivities are given on a logarithmic scale as a function of Q_z, since R_F decays proportionally to Q_z^{-4}. $R_F = 1$ below the critical momentum transfer, Q_c, if the scattering length density (SD) of the subphase, ρ_{bulk}, has a positive value. If $\rho_{bulk} < 0$, e.g., for neutron reflection from H_2O, Q_c is an imaginary quantity and R_F decreases monotonously with Q_z.

Data evaluation

In the general case, the reflectivity of an interface cannot be directly converted into the SD profile due to the loss of phase information in scattering experiments, although a model-independent reconstruction technique has been recently proposed (Zhou and Chen, 1993). Hence, the usual way to evaluate the data is to define and to refine an appropriate model. It has to be stressed that such a procedure does not lead to unique results. Rather, due to the phase problem, more than one set of parameters may yield *identical* reflectivities. In such cases it may be impossible to decide on the basis of reflectivity measurements alone which parameter set is the appropriate one.

For the calculation of the model reflectivities we have used the Parratt formalism (Parratt, 1954). Throughout this work we have used box models (see below) to describe the interface structure. For D_2O subphases the SD values were included as parameters in the fits. Fixed values for the surface roughness, $\sigma = 3$ Å (Vaknin et al., 1991c) for the lipid monolayer and $\sigma = 3.5$ Å (Vaknin et al., 1993) for protein/lipid layers, have been used and assumed to be equal at all interfaces for the evaluation of the model reflectivity. Within the narrow Q_z range accessible in measurements, the surface roughness has but a marginal influence on the model reflectivities. Similarly, fixed values, based on results from independent measurements, have been used for the lateral density and the hydrophobic layer thickness of chain-protonated lipids. These model parameters could not be determined from the neutron measurements, which implies that the model reflectivity is insensitive to them. Best-fit SD profiles have been determined using least-squares fitting to multiple data sets that were taken from isotopically distinct samples, as described below. The profiles were interpreted in terms of space filling molecular moieties.

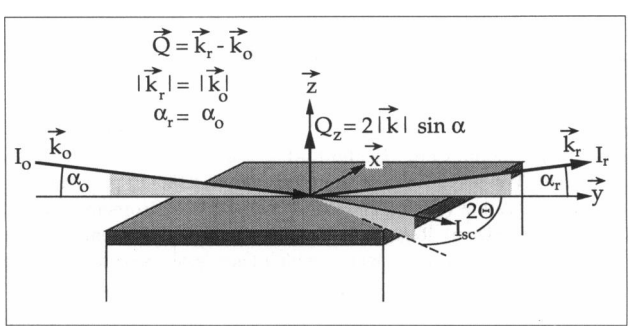

FIGURE 1 Schematic depiction of the geometry of a neutron or x-ray reflectivity measurement at a stratified interface. The impinging beam (intensity I_o, wave vector $\vec{k}_o$, incident angle α_o) is specularly reflected (I_r, $\vec{k}_r$, α_r). The momentum transfer, $\vec{Q}$, is strictly parallel to the surface normal $\vec{z}$. Off-specular scattering (intensity I_{sc}) at a horizontal scattering angle 2θ is also indicated.

Details of the model refinement

In an earlier investigation (Vaknin et al., 1991c) we described the structure of a lipid monolayer at an air/water interface using a two-slab model with five adjustable parameters. The information contained in one reflectivity data set was found to be insufficient in determining all five parameters with accuracy. We therefore developed an evaluation procedure which combined x-ray and neutron data from corresponding samples in a global data set, that was used for refinement of a generalized model (Vaknin et al., 1991b) under the assumption that the structures were identical in experiments with different radiation sources (x-ray or neutron) and, in neutron experiments, in samples with different isotopic constituents. The number of slabs of the model was chosen to correspond to the number of functional molecular parts in the system (Als-Nielsen and Kjaer, 1989), a hydrophobic layer next to the air and a hydrophilic layer incorporating the hydrophobic chains and the hydrated parts of the lipids plus water molecules, respectively. In the refinement procedure, the atomic content of these slabs was kept fixed while the packing conditions were adjusted under volume constraints. SD values were computed from the scattering lengths and the packing conditions, and the model was refined with all corresponding data sets *simultaneously*. A similar *composition-space refinement* technique has been independently developed to evaluate x-ray and neutron scattering data from vesicle suspensions (Wiener and White, 1991). Using this approach we have subsequently described protein/lipid layer systems (Vaknin et al., 1991a), where a third slab underneath the lipid accommodated the hydrated proteins.

In the present work we have adopted the following molecular interpretation of the interface structure (cf. Fig. 2): the lipid tail layer, closest to the air, comprised the hydrophobic moieties of the lipids. A comparison of the volumes of the disordered lipid chains from the fit with that of densely packed chains (Vaknin et al., 1991c) constituted a consistency check for the results. Underneath, the lipid head group layer incorporated a parameterized number of water molecules, n_w^{lhead}. Two biotin moieties per SA, conceived as protein bound, were included in the protein layer. This layer also incorporated a number of water molecules, n_w^{pr}. Thus, the volume associated with one SA molecule (area × thickness of the protein layer, $A_{pr} \times d_{pr}$) contained one SA, 2 biotins and n_w^{pr} water molecules and was located underneath $n_l = A_{pr}/A_l$ lipid molecules, which contained $n_l \times n_w^{lhead}$ water molecules in their head groups (see definitions in Table 1).

One critical set of parameters in the refinement was the volumes of the molecular constituents, and in particular that of SA, V_{SA}, since it dominates the SD of the protein layer. In our first report on neutron reflectivity experiments (Vaknin et al., 1991a) we overestimated V_{SA} from the x-ray crystal structure (Hendrickson et al., 1989) and, as a consequence, the quantitative conclusions on the amount of protein bound water were wrong. We were unable to discriminate between two distinct models of the interface which led to identical model reflectivities. We have since determined V_{SA} in combined x-ray and neutron reflection experiments on one particularly

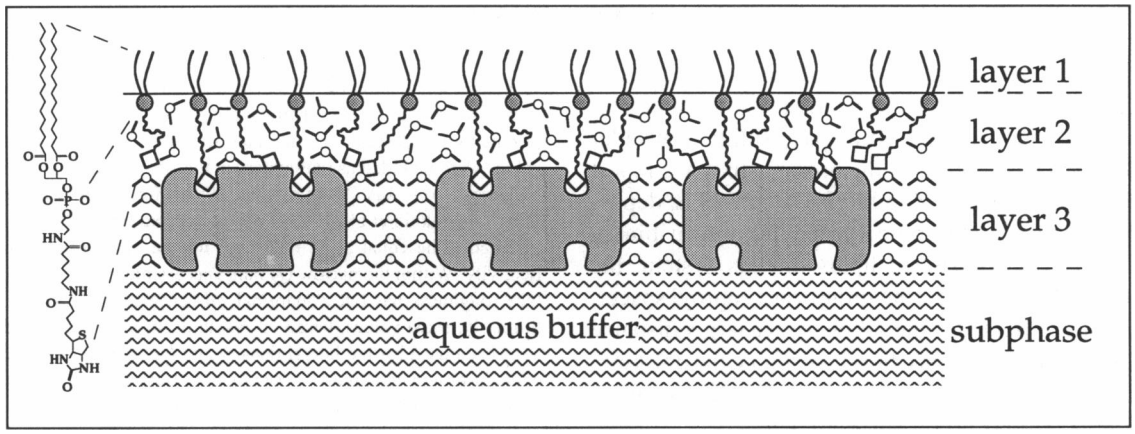

FIGURE 2 Molecular interpretation of the three-layer model used in this work. Layer 1, closest to the air, contains the hydrophobic moieties of the surface-deposited lipids. Layer 2 contains the hydrophilic moieties of the lipids, including the spacer-coupled biotins and hydration water molecules. Two biotins per protein, conceived as SA bound, are contained in layer 3, together with the hydrated protein. The molecular structure of the functionalized lipid is given in the inset.

TABLE 1 Best-fit parameters (two-box model) of the in situ structure of a biotinylated monolayer prior to protein binding. DMPC-d_{54}/B-cap-DPPE (3:1) at π = 15 mN/m, on 0.5 M NaCl in D_2O, $T \sim 18°C$

Parameter	Measurement	Description
Independent parameters		
A_1	85.8 Å^2	Area per lipid molecule in surface monolayer
d_{chain}	10.3 Å	Thickness of lipid tail group layer
d_{lhead}	7.2 Å	Thickness of lipid head group layer
Constants and dependent parameters		
σ*	3 Å	Surface roughness
n_w^{lhead}	6.3	Water molecules per (average) lipid head group

*Assumed from x-ray reflectivity data on lipid surface monolayers (Als-Nielsen and Kjaer, 1989).

well-investigated SA/lipid system (Vaknin et al., 1993). In the current study, the molecular volumes of the moieties of the system were obtained either from experiments (Vaknin et al., 1991c; Nagle and Wiener, 1988; Wiener and White, 1992) in the case of lipids; from computer models of molecular fragments (PM3 structure optimization starting from crystal structure data, with a subsequent estimate of the solvent-inaccessible volumes using the program MOLSV, QCPE program number QCMP053) in the case of the functionalized lipid; or from the bulk properties in the case of water and electrolytic solutions. The following numerical values were used: V_{SA} = 66,000 Å^3 (± 10% (Vaknin et al., 1993)); $V^{lhead}_{B\text{-}cap\text{-}DPPE}$ = 700 Å^3 (including biotin); V^{lhead}_{DMPC} = 335 Å^3; V_{biotin} = 227 Å^3; $V_{D_2O} = V_{H_2O}$ = 30 Å^3. The volume of the hydroxyl head group of cholesterol was neglected in the binary (3:1) mixture with B-cap-DPPE, i.e. the "average" head group volume was assumed to be 175 Å^3 (= 0.25 × $V^{lhead}_{B\text{-}cap\text{-}DPPE}$ + 0.75 × 0 Å^3).

The substrate scattering length densities accounted for the dissolution of 0.5 M NaCl. Since the repeated use of recycled D_2O lead to a continuous decrease in its isotopic purity, it was unpracticable to keep track of the pollution with H_2O at every stage of the experiments. We have therefore fitted the substrate SD of D_2O buffers in the modeling of the data.

Proton/deuteron exchange on the protein in isotopically different subphases was taken into account. The SA tetramer incorporates 828 exchangeable protons (for the amino acid composition of SA, see Green (1975)). While SA is perprotonated in H_2O buffer, a certain proportion of amino acids, which are readily accessible to solvent, will exchange deuterons for protons if the protein is dissolved in D_2O buffer. We have estimated the extent of this exchange from the experimental data on SA bound to binary mixtures of DMPC and B-cap-DPPE (see below). The data were best described if we assumed that $\delta \sim 60\%$ of the exchangeable protons are actually replaced by deuterons in D_2O buffer. We have subsequently used this value to describe the other experimental situations reported in this study.

Confidence limits of the best-fit parameters were evaluated by mapping the χ^2 "potentials" in the parameter space (Vaknin et al., 1991c): a P-dimensional set of independent parameters, $\tilde{a}$, of the model R was refined to its best-fit value, $\tilde{a}^{min}$, by finding the global minimum of

$$\chi^2(\tilde{a}) = \frac{1}{N-P}\sum_{i=1}^{N}\left[\frac{R_i - R(Q_z^i;\tilde{a})}{\sigma_i}\right]^2; \qquad \tilde{a} = \begin{pmatrix} a_1 \\ a_2 \\ \cdots \\ a_k \\ \cdots \\ a_p \end{pmatrix}, \qquad (1)$$

with respect to the N experimental reflectivity data R_i and their standard deviations σ_i which have been obtained at the momentum transfer values Q_z^i. To evaluate the sensitivity of the fit to changes in a parameter a_k from its optimum value a_k^{min}, Eq. 1 was minimized with respect to the remaining P-1 parameters while keeping a_k at a fixed value and readjusting χ^2 to a new local minimum. Since $\tilde{a}^{min}$ defined the global minimum in parameter space (at least in the range of parameters that is physically reasonable) this procedure mapped a potential-like situation with all values of the local minima in the (P-1)-dimensional space above the global minimum. We chose a 15% increase in χ^2 to define the confidence limit of the best-fit value of a parameter.

Materials and sample preparation

Samples were prepared on 0.5 M NaCl (p.a. grade, Merck, Darmstadt, Germany) solutions made from water that was either filtered (H_2O) in a Milli-Q apparatus (Millipore Corp., Bedford, MA; resistivity, Σ ~18 MΩcm) or distilled (D_2O) at least five times (four times from $KMnO_4$; p.a., Merck) in an all quartz/Teflon (PTFE) apparatus (Normag AG, Hofheim/Ts., Germany; Σ > 10 MΩcm). Resistivities were determined with a conductometer incorporated in the Milli-Q plant or with a hand-held apparatus (CG 858, Schott, Hofheim/Ts., Germany). The value given for our D_2O samples poses a lower limit. As judged from surface isotherms and from observing the dissolution of bubbles introduced into the H_2O or D_2O samples, their purity with respect to surface active compounds was comparable. The D_2O was stored in Teflon (FEP) bottles (Berghof, Eningen, Germany) and recycled after use. The isotopic purity of the D_2O was 94–98% in different experiments.

L-α-Perdeuterodimyristoylphosphatidylcholine (DMPC-d_{54}, purity > 99%; Avanti Polar Lipids, Alabaster, AL) and L-α-dimyristoylphos-

phatidylcholine (DMPC, > 99%) and cholesterol (>99%, both: Sigma, München, Germany) were used as supplied. These phospholipids were dissolved in $CHCl_3/CH_3OH$ (3:1; both solvents: p.a.; Merck). The biotinylated lipid *N*-biotinyl-S-{1,2-bis[(octadecyloxy)carbonyl]ethyl}cysteine (B-BOCEC; see Blankenburg et al. (1989)), used in previous investigations, was a generous gift from H. Ringsdorf, Mainz. B-BOCEC, *N*-biotinylcaproyldipalmitoylphosphatidylethanolamine (B-cap-DPPE, > 99%; Molecular Probes, Eugene, OR) and nitrobenzoxadiazolphosphatidylethanolamine (NBD-DPPE, >99%; Avanti) were dissolved in $CHCl_3$. For the preparation of binary lipid monolayers, lipid solutions were mixed before spreading.

For fluorescence experiments, streptavidin (Boehringer Mannheim, Penzberg, Germany) was labeled with fluorescein isothiocyanate (FITC, isomer I, Sigma) according to a standard procedure (Nargessi and Smith, 1986) with an average of two chromophores bound per protein molecule. To obtain a stock solution for neutron reflectivity experiments, the unlabeled protein was dissolved in a 0.5 M NaCl solution in D_2O at a concentration of 8 μM (0.5 mg/ml). For reflectivity experiments, 1-ml aliquots were injected into the electrolytic subphase of the film balance in the region of the illuminated surface. If no redistribution by convection or diffusion into the whole subphase volume (400 ml) is assumed, the amount of SA introduced is equivalent to less than 10 densely packed protein monolayers (limiting area per molecule in a protein monolayer estimated from Hendrickson et al. (1989): A_{SA}^{min} ~2,350 Å^2, cf. Vaknin et al. (1991a)). This amount was dissolved into a local aqueous depth of 300 μm. The actual protein/interface area ratio was smaller than the estimate given above, as traces of the protein were observed over the whole trough on cleaning after the experiments. Protein was usually injected underneath a lipid monolayer which had been prespread on a NaCl solution and had been characterized by reflectivity measurements; results were identical if a lipid monolayer was spread on a subphase that already contained the protein.

For electron microscopy, samples were prepared according to Darst et al. (1991) on a film balance under fluorescence microscopic control. Protein/lipid films were transferred to carbon-coated (~100 Å) grids at a lateral pressure, π = 30 mN/m, by touching the surface horizontally with the hydrophobic surface of the grid. Subsequently, the samples were flushed with Millipore water and soaked for ~30 s. with 1% (w/v) uranyl acetate solution. Reference experiments using micro-titer plates for the preparation of the sample instead of the film balance resulted in significantly poorer sample quality.

Instrumentation

Reflectometer

The neutron reflectometer located at the beam line TAS 7 of the DR3 reactor at Risø National Laboratory has been described in detail previously (Vaknin et al., 1991c). Cold neutrons delivered by the neutron guide are diffracted from the (002) planes of a highly oriented pyrolytic graphite monochromator at λ = 4.6 Å, confined by a variable slit-collimator-slit arrangement and impinge on the aqueous surface contained within a Langmuir film balance after passing a beam intensity monitor. The entrance angle onto the liquid interface, α_o, can be adjusted in the range between 0° and 7°. The coherence length is determined by the geometry of the reflectometer and is highly anisotropic in the plane of the specimen, ~10^5 and ~100 Å in $\tilde{y}$ and $\tilde{x}$ directions, respectively ($\tilde{y}$ is the direction of the projection of the beam, see Fig. 1).

The Langmuir film balance is encapsulated in a gas-tight and temperature-controlled aluminum container. Macroscopic surface waves are damped by a glass block submersed in the aqueous compartment underneath the beam. In this area the subphase depth is reduced to ~300 μm, which proved effective in preventing the propagation of accidentally excited surface waves. At the same time the subphase volume is considerably reduced for protein experiments. The illuminated area on the film balance is roughly kept constant at ~3 × 10 cm^2 by adjusting the slits during scans of α_o. Higher harmonics are removed from the reflected beam by a cooled beryllium filter. The background, both room background and incoherent scattering, is determined by rotating the detection arm of the instrument horizontally out of the specular position. As indicated in Fig. A2, the signal decays rapidly as a function of the rotation angle, 2θ. Experimentally, the background level is measured at $2\theta = \pm 3°$.

The instrument and data acquisition are computer-controlled. During measurement times for a reflectivity curve between $Q_z = 0$ and 0.3 Å^{-1} of typically 12 h, absolute reflectivity values as low as 10^{-6} can be determined after background subtraction. Radiation damage is negligible for both the x-ray and neutron measurements as indicated by the fact that results are reproducible after extended times of radiation exposure.

Fluorescence microscopy

Fluorescence microscopic measurements were performed in Mainz on a dedicated film balance with a microscope of local design incorporated into the bottom of the trough (Lösche and Möhwald, 1984). The instrument enables the measurement of the lateral distribution of dye molecules located at the interface with a resolution of ~2 μm. The chromophores may be directly attached to lipid molecules at the surface or, as in our experiments, bound to proteins that interact with the interface. In either case, only the emission from fluorophores with a distance from the surface less than ~1 μm is imaged. High sensitivity is achieved by using an SIT video camera head (C1000-12, Hamamatsu, Herrsching, Germany) to store data on tape (Super-VHS) or hard copy, and by standard on-line (Argus-10, Hamamatsu) and off-line (software: Image v1.28 by W. Rasband, National Institutes of Health, Bethesda, MD) image processing. Using FITC labels, approximately 1 chromophore per 10,000 Å^2 is sufficient to obtain micrographs with acceptable signal-to-noise ratio.

Electron microscopy

Electron micrographs were recorded with a Philips EM300 (low magnifications, ≤ 2,000 ×) on Ilford Pan F film (50 ASA) or with a Philips EM420ST (LaB_6 cathode at 100 kV; magnification, 60,000 ×) on 6 × 6-cm^2 photographic plates (Kodak ISO 163). Suitable regions on negative images were digitized using a CCD camera (Pullnix TM765 with Makro Nikkor f = 50 mm) with calibrated magnification, and subsequently Fourier-transformed on a computer (software: Image v1.28).

RESULTS

Synopsis of the investigated systems

In our previous work we have established the formation of a monomolecular layer of SA underneath a surface monolayer of the biotinylated lipid, B-BOCEC (Vaknin et al., 1991a), and have determined the solvent-inaccessible volume of the protein within the hydrated monolayer (Vaknin et al., 1993). This is a basis for an investigation of the structural organization of SA bound to different lipid surface monolayer systems in the current work. Here, we have used B-cap-DPPE as a functionalized compound with a longer spacer between the biotin and the head group, since the short spacer moiety in B-BOCEC ties the protein immediately to the surface-bound lipid, and it was anticipated that a longer spacer might improve the control over the structural organization. A fully extended head group of B-cap-DPPE is approximately 12 Å longer than that of B-BOCEC (see *inset* in Fig. 2). Besides the pure compound, we have investigated binary mixtures of B-cap-DPPE with DMPC, both with perprotonated and perdeuterated chains, and with cholesterol, on H_2O and on D_2O. Fig. 3 illustrates the relative neutron contrasts between the components of the systems.

The monolayers of the pure compound and the binary mixtures were compressed to a lateral pressure π = 3 and 15

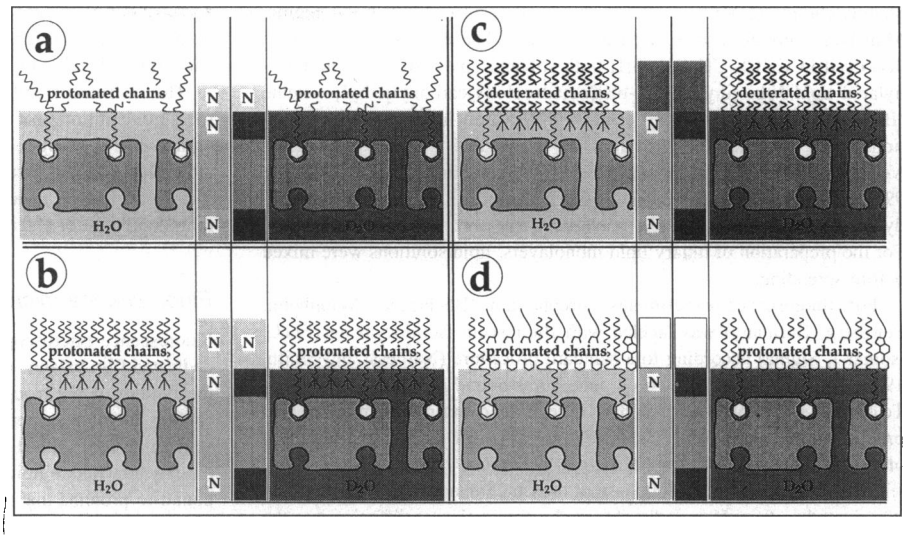

FIGURE 3 Cartoon of the investigated molecular lipid/protein layer systems. In the center columns of each panel grey scale representations of the SD contrast in the different layers are given. Negative values of the scattering length density are labeled "*N*." (*a*) SA underneath B-cap-DPPE at low lateral density in H_2O and D_2O. $\pi \sim 3$ mN/m. (*b–d*) Lipid monolayers consist of binary mixtures of fully protonated or chain-perdeuterated DMPC and B-cap-DPPE (*b* and *c*) or of cholesterol and B-cap-DPPE (*d*) on different subphases as indicated. $\pi = 15$ mN/m. All subphases contained 0.5 M NaCl.

mN/m, respectively. The areas per molecule at these pressures ensured a comparable biotin density at the interface and reduced steric hindrance between neighboring biotin moieties within the pure B-cap-DPPE lipid surface monolayers. We found that the lateral pressure of the monolayer did not increase significantly upon protein injection. Usually, a slight rise by less than $\Delta\pi = 3$ mN/m was observed in the course of 10 h, independent of the starting value of π. The final value of π was typically between 16 and 16.5 mN/m after 24 h if the protein was injected at 15 mN/m. The drift of the Wilhelmy balance was less than 0.3 mN/m in 24 h.

Measurements of reflectivity curves (R vs. Q_z) were only started after 2θ scans (see Fig. A2) had settled into a stable situation, usually 1–2 h after protein injection. 2θ scans were occasionally repeated after completion of the measurement of a reflectivity curve to ensure that no structural rearrangement had occurred during the duration of the experiment.

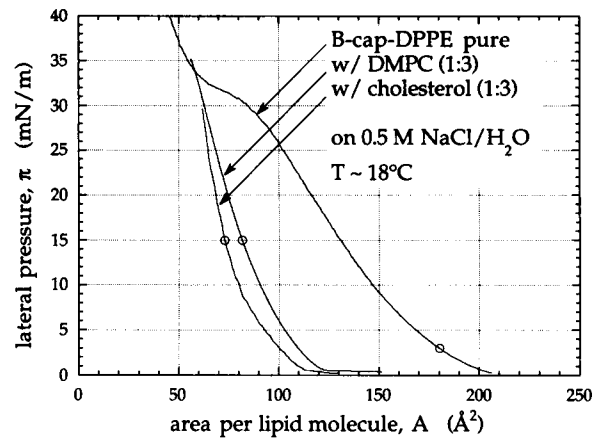

FIGURE 4 Surface monolayer isotherms, π vs. A, of B-cap-DPPE and its binary mixtures with DMPC and cholesterol (1:3) on 0.5 M NaCl in H_2O as the electrolytic subphase, $T \sim 18$°C. Same conditions as in the fluorescence microscopic and neutron reflectivity experiments, but no protein in the subphases. Marked are the points in the isotherm, where neutron reflectivity curves after SA binding have been measured.

Lipid monolayer isotherms

The general features of lipid surface monolayer isotherms are extensively discussed in the literature (Cadenhead et al., 1980; Bibo et al., 1991). Isotherms of the compounds and mixtures employed in this study are shown in Fig. 4. The isotherm of a B-cap-DPPE monolayer on 0.5 M NaCl in H_2O showed the same general features as the corresponding isotherm of B-BOCEC (cf. Fig. 3 in Blankenburg et al., 1989). At large areas, $A > 200$ Å^2 and $\pi \sim 0$ mN/m, the monolayer underwent a two-dimensional gas/liquid phase transition. At smaller areas, π rose gradually as the monolayer reached a homogeneous liquid phase. Decreasing the area to ~80 Å^2 drove the system into a first order phase transition from a more expanded to a more condensed phase, indicated by the plateau at $\pi \sim 30$ mN/m. At $A \sim 55$ Å^2 a homogeneous and highly condensed phase was reached as indicated by the low compressibility observed in the isotherm. The monolayer collapsed at $\pi \sim 45$ mN/m, $A \sim 45$ Å^2. The isotherm of B-cap-DPPE on D_2O was similar to the one on H_2O but showed a slightly increased lateral pressure. Here, the phase transition started at $\pi \sim 32$ mN/m, $A \sim 80$ Å^2 (data not shown).

Pure DMPC exhibits featureless isotherms at room temperature (Albrecht et al., 1978). The isotherms of chain-perprotonated and chain-perdeuterated DMPC monolayers on 0.5 M NaCl solutions in H_2O or D_2O were indistinguishable within experimental error (data not shown). In all cases, the lateral pressure of the monolayer rose steadily up to the collapse point without any indication of a phase transition within the condensed regime.

Isotherms of binary mixtures (3:1) of DMPC and B-cap-DPPE showed an almost ideal mixing behavior (Fig. 4). The onset of the lateral pressure upon compression was found at higher areas ($A \geq 110$ Å^2) than for pure DMPC monolayers due to the presence of B-cap-DPPE. A steady pressure increase upon compression was observed in the isotherms of all systems (data of the other mixtures not

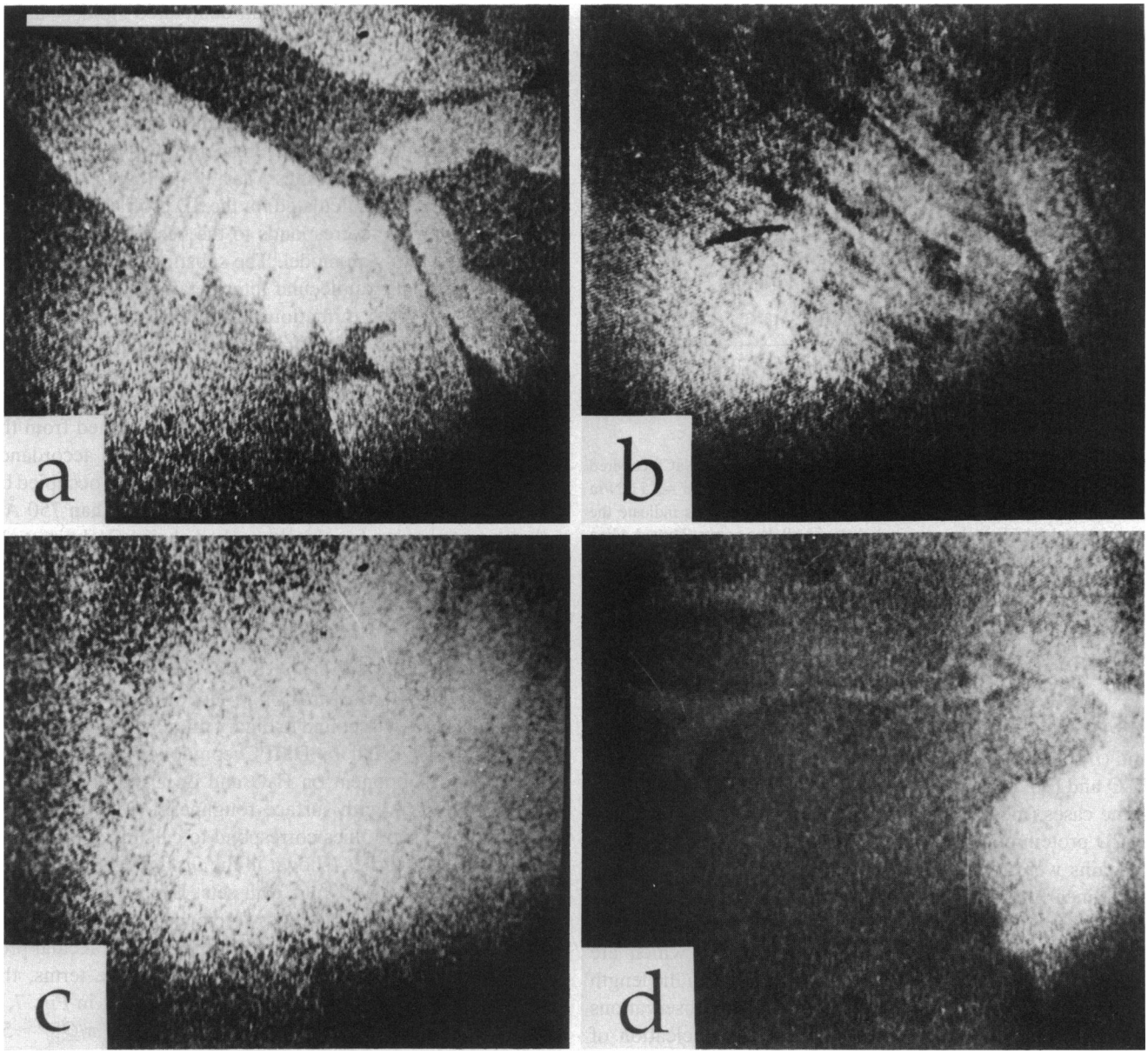

FIGURE 5 Fluorescence micrographs of FITC-labeled SA bound to binary mixtures (3:1) of perprotonated and chain-perdeuterated DMPC with B-cap-DPPE at 15 mN/m on different isotopic subphases containing 0.5 M NaCl, $T \sim 18°C$: (perprotonated) DMPC, H_2O (*a*) and D_2O (*b*); DMPC-d_{54}, H_2O (*c*) and D_2O (*d*). The bar in *a* represents 50 μm.

shown) up to $\pi \sim 40$ mN/m, where collapse occurred. The phase transition of the B-cap-DPPE component was barely visible at above 30 mN/m, and it could not be determined with accuracy whether or not a slight shift in the phase transition pressure occurred. No indication of a macroscopic phase separation was detected in fluorescence microscopic experiments in the condensed regime of the mixed monolayers (doped with 1 mol% NBD-DPPE). Isotherms of isotopically distinct systems could not be distinguished.

Similarly, featureless isotherms were observed with monolayers of binary mixtures of cholesterol and B-cap-DPPE (3:1) (see Fig. 4). The monolayer was slightly more condensed than that of the DMPC/B-cap-DPPE mixture, and no phase transition could be detected from its isotherm or from fluorescence microscopy.

Fluorescence microscopic observations of SA binding

Prior to neutron reflectivity measurements, the binding of FITC-labeled SA to functionalized lipid monolayers was characterized in fluorescence microscopic experiments with the systems depicted in Fig. 3. In all cases an interaction of the protein with the functionalized surface was indicated by a marked increase of the fluorescence from the interface region. Fig. 5 shows representative micrographs for the four different isotopic systems of the binary mixture DMPC/B-

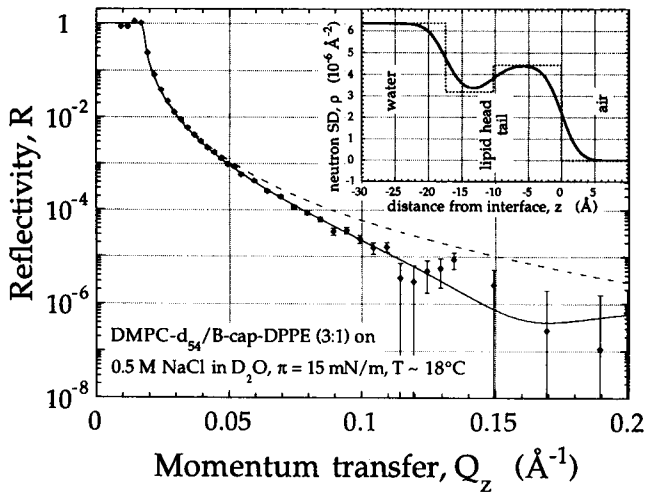

FIGURE 6 Neutron reflectivity of a D_2O subphase (0.5 M NaCl) covered with a binary mixture of DMPC-d_{54} and B-cap-DPPE (3:1) at $\pi = 15$ mN/m (A ~85 Å^2 per lipid molecule) and T ~18°C. The symbols indicate the experimental data. Error bars are included with all data points. The solid line is the computed reflectivity from the SD profile shown as a solid line in the inset. The dotted line in the inset indicates the box profile as it would appear without surface roughness. The parameters describing the model are listed in Table 1. The dashed line in the main figure indicates the substrate reflectivity with surface roughness.

cap-DPPE: (*a*) chain-protonated DMPC component on H_2O and (*b*) on D_2O; (*c*) chain-deuterated DMPC component on H_2O and (*d*) on D_2O. The scale bar in Fig. 5 *a* is 50 μm. In some cases (most clearly shown in Fig. 5 *a*), the formation of 2D protein domains at the interface was observed. These domains were optically anisotropic: the emission intensity after linearly polarized excitation depended on the polarization direction of the incident light. The differences in the morphological structures of different systems, which are shown in Fig. 5, may only be due to differences in the length scales of the inhomogeneities. Similar to the observations with B-BOCEC (Vaknin et al., 1991a), the nucleation of domains occurred faster on D_2O (Fig. 5 *b*) than on H_2O (Fig. 5 *a*), leading to domains that were too small to be clearly imaged in the fluorescence microscope. With lipid mixtures involving DMPC-d_{54} (Fig. 5, *c–d*), the features were generally more fuzzy, and we did not observe a pronounced optical anisotropy of the structures which would be suggestive of a crystalline state.

SA binding to surface monolayers of pure B-cap-DPPE ($\pi = 3$ mN/m) resulted in macroscopic morphologies similar to those shown in Fig. 5 *a*, whereas under monolayers of the cholesterol/B-cap-DPPE mixture at $\pi = 15$ mN/m structures were similar to those in Fig. 5 *b* (data not shown).

Neutron reflectivity measurements

Lipid surface monolayers

Some of the lipid monolayers were characterized by neutron reflection measurements prior to protein injection into the subphase. The fully protonated samples add virtually no contrast to the scattering length density profile of the bare interface. Conversely, with chain-deuterated lipids, surface monolayers show sufficiently high contrast for structural investigations. Fig. 6 shows the neutron reflectivity of a binary monolayer of DMPC-d_{54}/B-cap-DPPE on D_2O/NaCl observed over a range of almost seven orders of magnitude. Included with the data are the Fresnel reflectivity of the subphase (with surface roughness) as a broken line and as a full line the reflectivity calculated for the SD profile shown in the inset. This profile corresponds to the best-fit parameter set describing a two-slab model. The substrate SD has been included in the fit. A molecular interpretation of this profile is consistent with the formation of a hydrophobic lipid chain layer (thickness: d_{chain} ~10.3 Å) on top of a hydrophilic lipid head group slab (thickness: d_{head} ~7.2 Å). Approximately 6 D_2O molecules are associated with each lipid head group. The density of the lipid monolayer, as determined from the neutron data, is about 1 molecule per 86 Å^2, in accordance with the isotherm. The resulting average volume occupied by the lipid tails is ~880 Å^3, considerably larger than 750 Å^3, the expected value for closely packed chains (Vaknin et al., 1991c). The best-fit values are listed in Table 1.

Protein monolayers adsorbed to binary DMPC/B-cap-DPPE mixtures

Fig. 7, *a–d*, shows the neutron reflection from buffer interfaces where SA was bound to binary mixtures of DMPC with B-cap-DPPE (*a* and *b*: DMPC component and *c* and *d*: DMPC-d_{54} component on H_2O and on D_2O). The Fresnel reflectivities R_F (with surface roughness) are indicated by broken lines; solid lines correspond to calculated reflectivities using SD profiles (shown in the *insets*) deduced from a simultaneous fit to all four data sets. Even when analyzed individually, i.e., without cross-reference to one another, all four data sets indicated the formation of monomolecular protein layers underneath the lipid. In qualitative terms, the minima in reflectivity around Q_z^{min} ~0.065 Å^{-1} in Fig. 7, *b* and *d*, are related to the total film thickness $d \sim \pi/Q_z^{min}$ ~50 Å (Als-Nielsen and Kjaer, 1989; Tidswell et al., 1990; see also Eq. A11). None of the individual data sets is sufficient to support a three-layer model. However, combining the four data sets and fitting to them one general model simultaneously necessitated a three-layer description.

The best-fit values are listed in Table 2. The protein monolayer had a thickness $d_{pr} = 40 \pm 4$ Å; one SA molecule with its associated water molecules occupied an area $A_{pr} = 3{,}300 \pm 300$ Å^2 within the protein film.[1] These results imply that

[1] To address the question if contrast variation has an influence of its own on the self-assembled structure we have also modelled the data with different parameters $A_{pr}^{H_2O}$ and $A_{pr}^{D_2O}$ in order to account for microscopic differences in the protein organization, which could be the reason for the macroscopic morphology differences in the fluorescence microscopic observations: a smaller size of the 2D protein domains on D_2O than on H_2O may be due to a higher nucleus density, and hence a smaller size of critical nuclei (Adamson, 1990). This would indicate a larger gain in the free energy associated with the incorporation of a surface-bound SA molecule into a domain, connected with a smaller average distance between neighboring SA molecules, and hence a smaller value A_{pr}. We found that $A_{pr}^{H_2O}$ and $A_{pr}^{D_2O}$ were identical

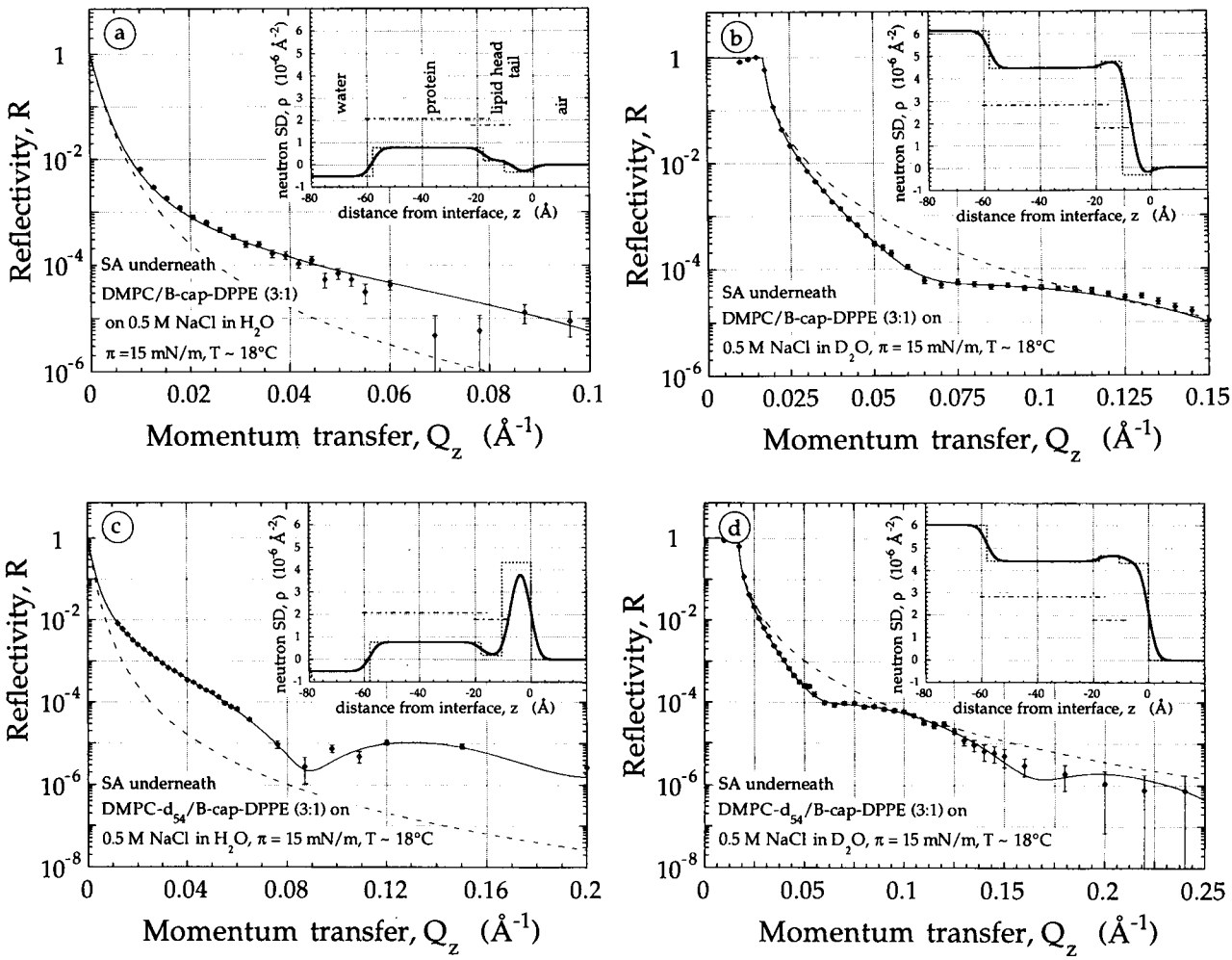

FIGURE 7 Neutron reflectivities of aqueous surfaces with SA bound to binary DMPC/B-cap-DPPE (3:1) monolayers on 0.5 M NaCl in water at various contrasts (π = 15 mN/m, T ~18°C). The different panels correspond to the experimental situations shown in Fig. 3, *b* and *c*. The solid lines are the computed reflectivities from the best-fit models of a simultaneous refinement procedure (see text). The corresponding SD profiles are included as insets and the model parameters are listed in Table 2. Dashed-dotted lines in the insets indicate the SD expected for dry SA and for the dehydrated lipid head groups. Note the difference in the SDs of SA on H_2O and D_2O due to the exchange of protons.

SA constituted 58 ± 3 wt% of this slab. With V_{SA} = 66,000 Å^3 (Vaknin et al., 1993), the data were best described if we assumed that about 60% of the exchangeable protons on the SA tetramer were displaced by deuterons from the D_2O buffer. However, the fraction of exchanged protons, δ, could only approximately be determined, since it is correlated with V_{SA} and the uncertainty in V_{SA} inferred a large uncertainty in δ. We estimate δ = 60% ± 40%.

The area per phospholipid molecule at the surface increased from 85 to 120 Å^2, indicating that the monolayer was severely rearranged by the protein application and incubation. In order to quantify the effect of SA binding on the in-plane homogeneity of the interface structure we compared the shape of the diffuse scattering from the surface before and after protein binding by detuning the specular angle α_r. As an example, Fig. 8 shows scans of the reflection angle α_r (cf. Fig. A1) around the specular reflection position from a DMPC-d_{54}/B-cap-DPPE monolayer on D_2O prior to and after protein injection. The half widths of the intensity peaks are identical within experimental error suggesting that the molecular protein layer was homogeneous on a length scale greater than the coherence length of the probing beam in Q_y direction (10 μm).

Protein monolayers adsorbed to pure B-cap-DPPE monolayers

Fig. 9 shows the neutron reflectivity of buffer interfaces with SA bound to pure B-cap-DPPE monolayers on (*a*) H_2O and on (*b*) D_2O. Insets show SD profiles obtained from the simultaneous refinement of the data sets. Both data sets on their own were consistent with the formation of monomolecular protein layers underneath the lipid surface monolayers. The slight shift in the minimum position in the D_2O data set to Q_z^{min} ~0.075 Å^{-1} with respect to the binary mixtures

within experimental error. Similarly, different parameters $A_{pr}^{CH_2}$ and $A_{pr}^{CD_2}$ resulted in identical best-fit values.

TABLE 2 Best-fit parameters (three-box model) of the in situ structure of streptavidin bound to a biotinylated monolayer, DMPC/B-cap-DPPE (3:1) at π = 15 mN/m, at the air-buffer (0.5 M NaCl) surface, $T \sim 18°C$

Parameter	Measurement	Description
Independent parameters		
A_{pr}	3,300 ± 300 Å^2	Average area per protein
(A_{pr}^{EM}	3,400 ± 700 Å^2	Area per protein from electron micrographs)*
d_{pr}	40.0 ± 4 Å	Protein layer thickness
A_1	121 ± 12 Å^2	Area per lipid molecule in surface monolayer
d_{chain}	7.5 ± 3 Å	Thickness of lipid tail group layer
d_{lhead}	10.5 +2.5/–4.0 Å	Thickness of hydrated lipid head group layer
Constants and dependent parameters		
σ‡	3.5 Å	Surface roughness
V_{SA}‡	66,000 Å^3	Water-excluded volume of SA in the film
n_w^{pr}	2,200 ± 300	Water molecules per SA in the protein film
n_w^{lhead}	29.0 ± 6	Water molecules per (average) lipid head group
n_1	27 ± 4	Lipids in surface monolayer per protein
Scattering length densities and volume constraints (b_i are the nuclear neutron scattering lengths)		
ρ_{pr}	$= (b_{SA} + n_w^{pr} b_w + 2b_{biotin})/A_{pr} d_{pr}$	Protein layer
ρ_{lhead}	$= ((b_{head}(avg.) + n_w^{lhead} b_w) n_1 - 2b_{biotin})/A_{pr} d_{lhead}$	Lipid head group layer
ρ_{chain}	$= b_{chain}(avg.)/A_1 d_{chain}$	Lipid tail layer
n_1	$= A_{pr}/A_1$	
n_w^{lhead}	$= (A_{pr} d_{pr} - V_{SA} - 2V_{biotin})/V_w$	
	$= (A_{pr} d_{lhead} - n_1 V^{lhead}(avg.) + 2V_{biotin})/V_w n_1$	

The volume ($A_{pr} \times d_{pr}$) of the protein compartment comprises one SA molecule (volume V_{SA}), n_w^{pr} water molecules (V_w = 30 Å^3), and two biotin head groups (V_{biotin} ~227 Å^3).

*Value given for comparison.

‡From experimental data (Vaknin et al., 1993).

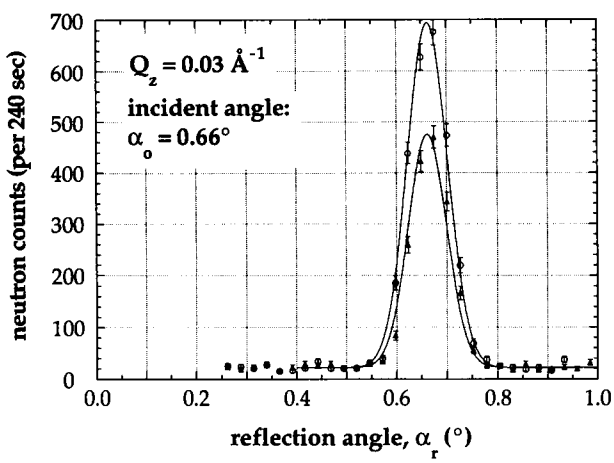

FIGURE 8 Reflected neutron intensity as a function of α_r at constant α_o from a DMPC-d_{54}/B-cap-DPPE monolayer on D_2O/NaCl prior to (*circles*) and after (*triangles*) SA binding. The solid lines are Gaussian fits to the data. Half widths of the reflection peaks are identical within experimental error.

(Fig. 7, *b* and *d*) indicates a decrease in the overall layer thickness of the interface structure to about 45 Å.

We have analyzed the data with a three-layer model, in order to enable a direct comparison with the results for the binary lipid mixtures with DMPC. However, an analysis of the nuclear scattering lengths of the constituents shows that this concept reduces effectively to a two-layer description (see also *insets* in Fig. 9): the perprotonated lipid chains add virtually no scattering length to the profile. Moreover, the contribution of the lipid head group slab is much smaller than that of the hydrated protein film. We have therefore *assumed* a layer thickness d_{chain} = 10 Å, slightly larger than that in the binary mixture, but significantly smaller than the value determined for DPPC-d_{62} at π = 42 mN/m (Vaknin et al., 1991c), and have kept this value constant during the data evaluation. The surface monolayer area, which could not be determined from neutron reflectivity measurements due to the lack of contrast, was assumed to be A_1 = 130 Å^2/molecule from the isotherm, and kept constant in the fit. In contrast, the thickness and the hydration of the lipid head group slab were refined in the model. Our assumption that the structure of the lipid monolayer was not changed by the protein application and incubation, despite the structural changes which we have been able to quantify for the DMPC mixtures, does not affect the conclusion on the structure of the protein aggregate and affects the lipid head group only with respect to its hydration, since the measurement is sensitive to the *total amount* of water in that slab. The general conclusions on the structural properties of the layer system are independent of A_1.

The results from the model refinement are listed in Table 3. The uncertainties of the determined parameters are small compared to those determined for the binary lipid mixtures with phosphocholines due to the fact that we have used assumptions on A_1 and d_{chain}. Qualitatively, we can draw the following conclusions from a comparison to the structural organization of the system with the binary lipid mixture in the surface monolayer: (*a*) the protein was organized in a more compact structure. One protein molecule occupied an average area of A_{pr} ~2,900 Å^2 and had ~1,600 water molecules associated with it. We thus observed a significantly higher protein density at the interface (~66 wt% of SA in the hydrated monolayer on H_2O buffer); (*b*) the lipid's head

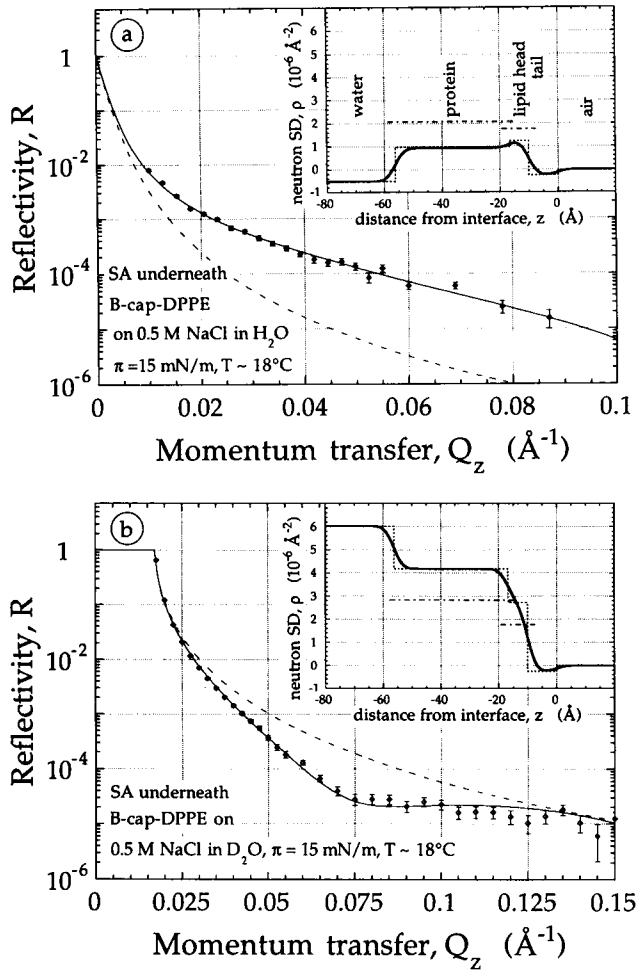

FIGURE 9 Neutron reflectivity of aqueous surfaces with SA bound to pure B-cap-DPPE monolayers, cf. Fig. 3 *a*, on 0.5 M NaCl in water at two contrasts (π ~3 mN/m, T ~18°C). The solid lines show the computed reflectivities from the best-fit models of a simultaneous refinement procedure. The corresponding SD profiles are included as insets and the model parameters are listed in Table 3.

group was dehydrated. We measured ~5 water molecules attached to each lipid head group, compared with ~30 water molecules that were included in the head groups of the phospholipid mixture; (*c*) the thickness of the protein layer, d_{pr} ~40 Å, was identical within experimental error in both cases.

Protein monolayers adsorbed to binary cholesterol/ B-cap-DPPE mixtures

The neutron reflectivity from buffer interfaces with SA adsorbed to surface monolayers of binary mixtures of cholesterol with B-cap-DPPE are shown in Fig. 10. A pronounced minimum in the reflectivity is observed at Q_z^{min} ~0.075 Å^{-1}, suggesting a total width of the interface structure of about 45 Å. The protein was organized in monomolecular layers under the functionalized lipid. Simultaneous refinement of both data sets led to the SD profiles shown in the insets. These demonstrate that the three-layer model formally used reduces practically to a two-layer model. The reason is that the 3:1 mixture of cholesterol and B-cap-DPPE shows a exceedingly small scattering length per (average) hydrophobic moiety of the lipid monolayer (2.38 × 10^{-6} Å, compared with 3.92 × 10^{-3} Å for the binary mixture DMPC-d_{54}/B-cap-DPPE). To be consistent with the models for the other investigated lipid systems, we have formally included this minute scattering length in the fit in a "three"-slab model. The area per lipid molecule was determined from the isotherm, A_l = 75 Å^2, and kept constant in the fit. The parameter set which fitted the data best, cf. Table 4, suggests thicknesses of the protein layer of d_{pr} ~36 Å and of the lipid head group layer of d_{lhead} ~10 Å. Although the result for d_{pr} is somewhat small, it agrees with the other results within experimental error. One SA molecule occupied an average area of A_{pr} ~2,800 Å^2 and was hydrated by ~1,100 water molecules (~74 wt% of SA in the hydrated monolayer on H_2O). Whereas the density of the protein layer was comparable with the results from the systems with the pure B-cap-DPPE surface monolayer, significantly more water, ~20 molecules per lipid, was observed in the head group slab.

Electron microscopy

For a few samples, electron microscopy (EM) experiments were conducted in order to cross-check the protein density obtained from neutron reflectivity experiments. Fig. 11 shows a typical transmission electron micrograph of an uranyl stained SA layer attached to DMPC/B-cap-DPPE (3:1) at low magnification (scale bar: 5 μm). We compressed the surface monolayer to π = 30 mN/m prior to protein adsorption in the preparation procedure, since the samples did not transfer well at 15 mN/m.

It is easy to discriminate between protein covered (i.e., stained) and uncovered areas in the micrograph. Due to the mechanical stress upon transfer, the film was ruptured, and multiple cracks are seen in the image. Nevertheless, large areas of the order of tenths of μm^2 have been transferred intact and could be further investigated in high-magnification EM. The results showed that these regions are probably not comprised of single 2D SA crystals, but positional correlation was observed in areas larger than 100 × 100 nm^2. Fig. 12 *a* shows an image of such an area (scale bar: 1000 Å). The primary magnification in the EM was 60,000×. A well-ordered stripe-pattern is visible on close inspection of the micrograph. Such micrographs were digitized into a matrix of 512 × 512 pixels, and Fourier-transformed on a computer. The resulting Fourier space representation of a 166 × 166 nm^2 area of Fig. 12 *a* is shown in Fig. 12 *b*. It is assumed that all the observed reflections are due to one 2D crystal contained within the digitized image, because no grain boundaries or changes in orientation of the lattice could be detected in the real space image. The Fourier map is compatible with an oblique lattice (γ ~68°). First and second order Fourier peaks are observed in the transform at about k = (45 ± 4 Å)$^{-1}$ (Fourier peak *A*); (25 ± 3 Å)$^{-1}$ (*E*); (42.2 ± 4 Å)$^{-1}$ (*B*); (81 ± 6 Å)$^{-1}$ (*D*); and (26.2 ± 5 Å)$^{-1}$ (*C*). Reflection *D* could not be identified in all cases on the trans-

TABLE 3 Best-fit parameters for the in situ structure of streptavidin bound to a biotinylated monolayer, B-cap-DPPE at π = 3 mN/m, at the air-buffer (0.5 M NaCl) surface, $T \sim 18°C$

Parameter	Measurement	Description
Independent parameters		
A_{pr}	2,900 ± 150 Å^2	Average area per protein
d_{pr}	39.5 ± 4 Å	Protein layer thickness
d_{lhead}	6.7 ± 2 Å	Thickness of hydrated lipid head group layer
Constants and dependent parameters		
V_{SA}*	66,000 Å^3	Water-excluded volume of SA in the film
A_1‡	130 Å^2	Area per lipid molecule in surface monolayer
d_{chain}	10 Å	Thickness of lipid tail group layer
σ*	3.5 Å	Surface roughness
n_w^{pr}	1,600 ± 200	Water molecules per SA in the protein film
n_w^{lhead}	6.5 ± 8	Water molecules per lipid head group
n_1	22.5 ± 1	Lipids in surface monolayer per protein

It was assumed that ~60% of the exchangeable protons on SA were replaced by deuterons on D_2O. For more details, see Table 2.
* From experimental data (Vaknin et al., 1993).
‡ From the isotherm.

forms from different real space images. Assuming that the innermost reflections, *A* and *D*, define the fundamental vectors (1, 0) and (0, 1), the unit cell area is A_{uc} ~3,380 ± 700 Å^2. The remaining reflections may then be indexed as *B*: (0, 2); *C*: (−1, 3); and *E*: (2, 0).

In a more elaborate investigation of similar transferred SA/lipid layer systems, where the protein was bound to B-BOCEC in binary mixtures with an unsaturated phosphocholine, Darst found a size of the rectangular unit cell of 80 × 85 Å^2 (Darst et al., 1991). Two SA molecules were contained within this unit cell. From this result, and with an estimate of the lower limit for the area per SA of 2,350 Å^2 (from Hendrickson et al. (1989), see Vaknin et al. (1991a)), we conclude that the unit cell in the present study contains just one protein molecule. We estimate the area per SA molecule within the transferred and stained structure therefore to be A_{pr}^{EM} = 3,400 ± 700 Å^2 in the protein layer bound to the 3:1 mixture of DMPC and B-cap-DPPE (see Table 2), comparable to the value determined in the in situ neutron reflectivity measurements.

DISCUSSION

In previous work (Vaknin et al., 1991a; Lösche et al., 1992; Lösche, 1992; Vaknin et al., 1993) we have demonstrated how to extract structural information on the molecular length scale from reflectivity measurements on self-assembled protein interface layers. Here, we use neutron reflectivity as well as electron and fluorescence microscopy to investigate how the structural organization of such supramolecular interface layers is influenced by surface chemistry. In combination with the data reported in our earlier work with the functionalized lipid B-BOCEC (Vaknin et al., 1993) our results show two trends in how the protein organization responds to changes in the chemical composition of the functionalized surface monolayer, and from these trends we postulate that:

(1) *the lateral protein density depends on the 'effective' spacer length between the biotin and its hydrophobic anchor on the functionalized lipid.*

The effective spacer length is that part of the spacer moiety, which is not impeded in its mobility by steric hindrance from neighboring head groups of nonfunctionalized lipids. When bound to pure monolayers of B-BOCEC (Vaknin et al., 1993), where biotin is directly attached to a small head group, SA was found to organize in a low density at the interface, approximately 1/4,600 Å^{-2}. In contrast, upon binding to B-cap-DPPE and to cholesterol/B-cap-DPPE mixtures, where the spacer length is increased by ~12 Å, we observed a considerably larger density, approximately 1/2,800 Å^{-2}. Due to the size of the cholesterol head group the flexibility of the spacer on B-cap-DPPE is not reduced in the binary mixture, so that the effective spacer length is the same in both cases. The spacer's flexibility in this binary mixture may even be increased, since the interdispersion of cholesterols between the functionalized lipids will reduce steric hindrance, which neighboring B-cap-DPPE head groups exert upon one another in pure monolayers.

In comparison, mixing B-cap-DPPE with DMPC leads to a reduction in the effective spacer length, since the choline head groups are much bulkier than those of cholesterol and reduce the mobility of a large part of the spacer on B-cap-DPPE. In condensed lipid surface monolayers, the choline head groups were found to extend to about 9 Å from the interface (Vaknin et al., 1991c). In response, the bound protein organizes in a slightly decreased lateral density at the interface, 1/3,300 Å^{-2}. The reason for only a moderate protein density reduction may be that those parts of the spacers, which extend further away from the interface than the choline head groups, are higher in their mobility than they would be in pure B-cap-DPPE monolayers, where they are subject to mutual head group interference.

We speculate that the length and the flexibility of the spacer control the flexibility of an individual surface bound SA molecule to adjust to one another in order to form the arrays of surface immobilized proteins observed in fluorescence and electron microscopy. As has been demonstrated with electron microscopy, there exists long-range positional order within these protein domains, although such aggregates are most likely not just 2D crystals in a classical sense (Haas and Möhwald, 1993). Since the

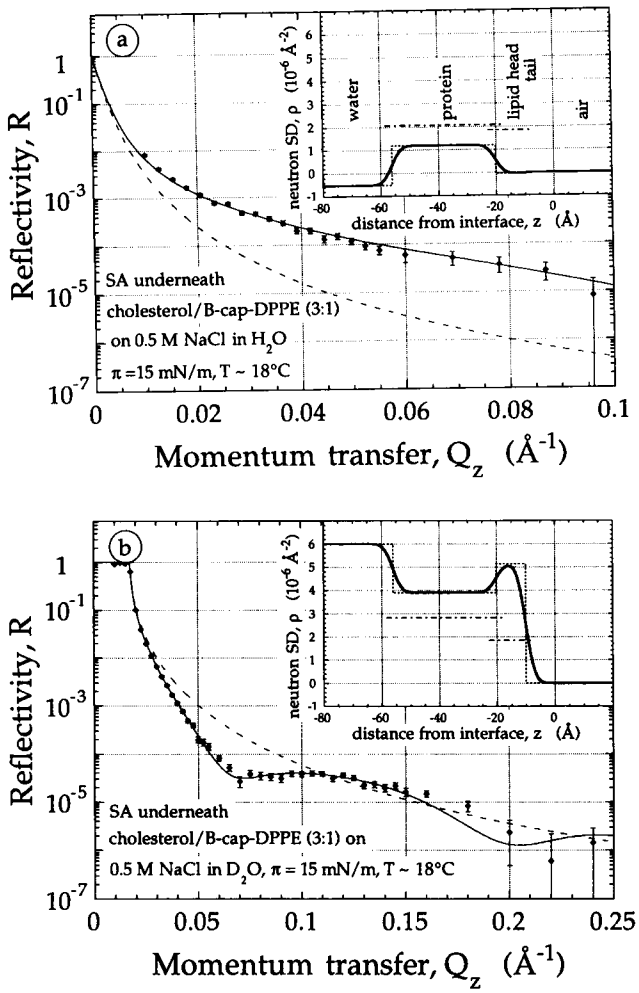

FIGURE 10 Neutron reflectivity of aqueous surfaces with SA bound to binary cholesterol/B-cap-DPPE (3:1) monolayers, c.f. Fig. 3 *d*, on 0.5 M NaCl in water at two contrasts (π = 15 mN/m, T ~18°C). The solid lines show the computed reflectivities from the best-fit model of a simultaneous refinement procedure. The corresponding SD profiles are included as insets and the model parameters are listed in Table 4.

nucleation and growth of such 2D domains are collective processes, it seems reasonable to assume that the manner in which a surface-bound protein is actually ligated to the interface, may control the density of proteins in the aggregates.

(2) *The dipole moment density at the interface controls the amount of water which interpenetrates the protein and lipid monolayers.*

Whereas in monolayers of the pure components the slightly hydrophobic head groups of the functionalized lipids are dehydrated in the protein bound state ($n_w^{lhead} \leq 5$ for both B-BOCEC and B-cap-DPPE), a large number of water molecules is observed between the lipid and protein monolayers with both binary B-cap-DPPE mixtures ($n_w^{lhead} \geq 15$ for cholesterol and $n_w^{lhead} \geq 25$ for DMPC). The dipole moment associated with the hydroxyl head group of cholesterol is significantly smaller than that of the choline head group. As in the case of the protein density, it seems intuitively clear what one should expect as a response of the system to the inferred chemical changes, but only by reflectivity measurements it was possible to quantify the structural changes in the protein organization at the interface.

In all cases which we have studied are the values of the protein layer thicknesses at the interface identical within experimental error. d_{pr} ~40 Å suggests that SA binds with its smallest edge parallel to the interface normal. In the crystal structure, the projection of this edge on the local axis is ~48 Å in length (Hendrickson et al., 1989). The fact that we measure a thickness of the bound protein layer smaller than that does not indicate that the interface is only partially covered with protein, but that we measure the average thickness of a bumpy structure, which may even partially interpenetrate the lipid surface monolayer if bound via a short spacer as in the case of B-BOCEC (Vaknin et al., 1993). Correlating the orientation of the surface bound protein with its crystal structure confirms that the protein presents two binding pockets toward the interface, and hence its two remaining binding sites toward the bulk of the subphase. This suggests that SA binds to two receptor molecules at the surface and is the structural basis for the capability of the SA monolayer to bind dissolved biotinyl derivatives from the fluid phase, and thus to form complex, but well-defined, supramolecular structures (Herron et al., 1992).

In the discussion of protein interaction with interfaces, unspecific adsorption is invariably a major issue. It is therefore worth stressing that in preparations where the protein would not be specifically adsorbed, the neutron and fluorescence microscopy data (not shown) gave no indications for the presence of protein at the interface. Based on neutron data (not shown), the protein formed the same interface structures after injection underneath a preformed biotinylated lipid monolayer and upon spreading of the biotinylated lipid on a protein solution.

We have addressed the question of whether isotopic contrast variation has an impact of its own on the *average* microscopic structure (see explanatory footnote in Results) and have not found any indication that it does. In particular, we see no influence on the protein density at the interface. This is not trivial, since from nucleation theory (Adamson, 1990) the observed differences in the macroscopic morphologies of the 2D protein aggregates on H_2O and D_2O subphases might be expected to reflect microscopic morphology differences (Vaknin et al., 1993).

In our model we have assumed that the surface is covered with a laterally homogeneous structure. This assumption collides apparently with the fluorescence microscopic observation that the protein organizes in macroscopic 2D domains at the interface which are interdispersed with a continuous phase, that has presumably a different microscopic structure. In contrast to the emission from the domains, the fluorescence from the continuous phase is isotropic, indicative of a higher symmetry. This does not necessarily imply a lower protein density: although anisotropic domains occupy a high

TABLE 4 Best-fit model (quasi-two-box model) for the in situ structure of streptavidin bound to a biotinylated monolayer, cholesterol/B-cap-DPPE (3:1) at π = 15 mN/m, at the air-buffer (0.5 M NaCl) surface, $T \sim 18°C$

Parameter	Measurement	Description
Independent parameters		
A_{pr}	2,800 ± 125 Å^2	Average area per protein
d_{pr}	35.8 + 4.5/–3.5 Å	Protein layer thickness
d_{lhead}	10.2 ± 2 Å	Thickness of lipid head layer
Constants and dependent parameters		
V_{SA}*	66,000 Å^3	Water-excluded volume of SA in the film
A_1‡	75 Å^2	Area per lipid molecule in surface monolayer
d_{chain}	10 Å	Thickness of lipid tail group layer
σ*	3.5 Å	Surface roughness
n_w^{pr}	1,100 + 300/– 250	Water molecules per SA in the protein film
n_w^{lhead}	20 ± 5	Water molecules per lipid head group
n_1	37.5 ± 1.5	Lipids in surface monolayer per protein

It was assumed that ~60% of the exchangeable protons on SA were replaced by deuterons on D_2O. For more details, see Table 2.
*From experimental data (Vaknin et al., 1993).
‡From the isotherm.

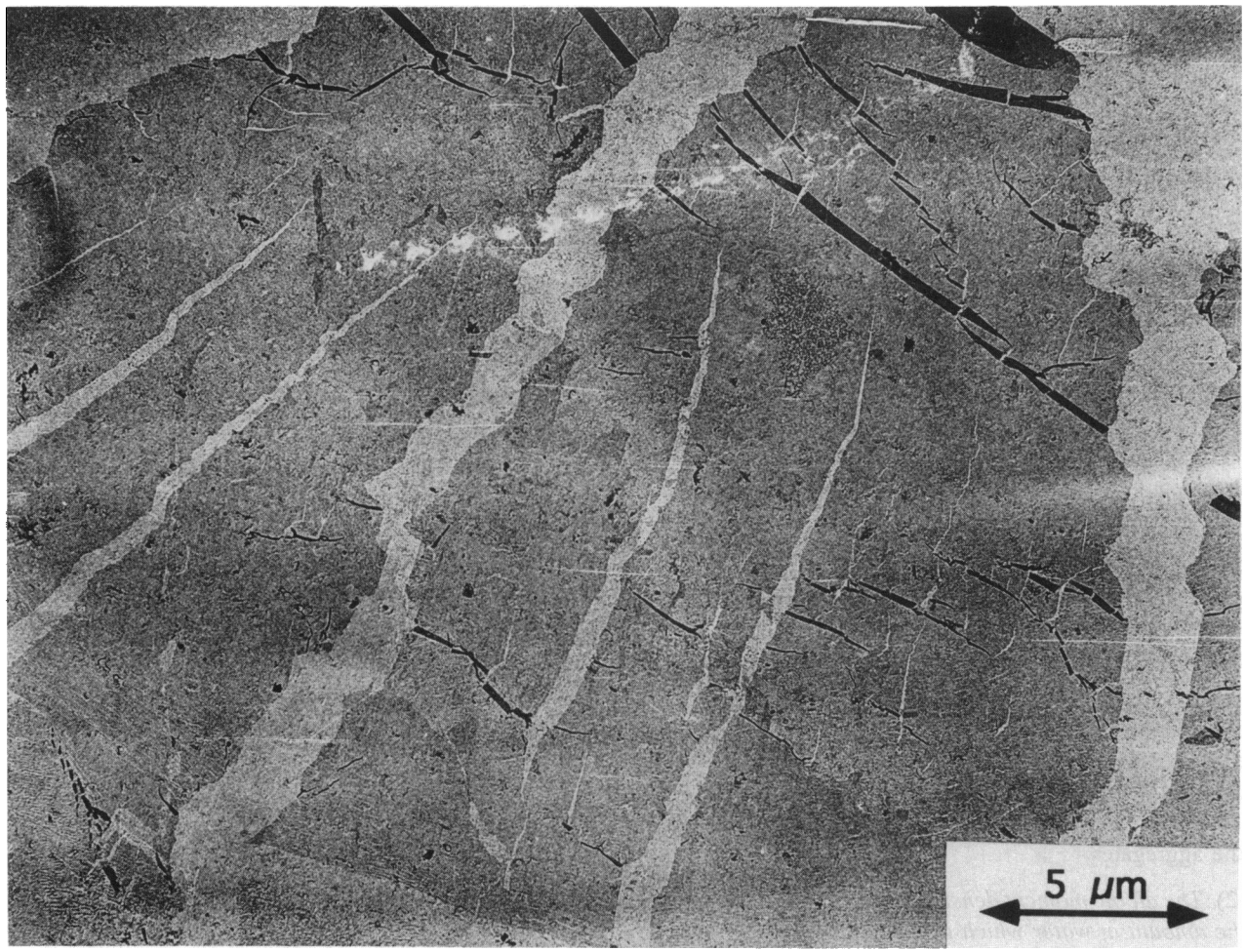

FIGURE 11 Transmission electron micrograph of a SA monolayer bound to a binary DMPC/B-cap-DPPE monolayer at π = 30 mN/m, T ~18°C, transferred to a carbon-coated electron microscopy grid and stained with 1% uranyl acetate. The scale bar is 5 μm.

proportion, ~90%, of the surface area under lipid monolayers of B-BOCEC (Lösche et al., 1992; Vaknin et al., 1993) we observed a lower protein density than in the cases reported here. In the systems investigated here, the macroscopic surface structure as reported from fluorescence microscopy depends strongly on the isotopic constitution both of the subphase buffer and the lipid chains (cf. Fig. 5). On the other side we have some evidence that the average microscopic structure is similar within the frame of the model in isotopically distinct preparations, as inferred from model

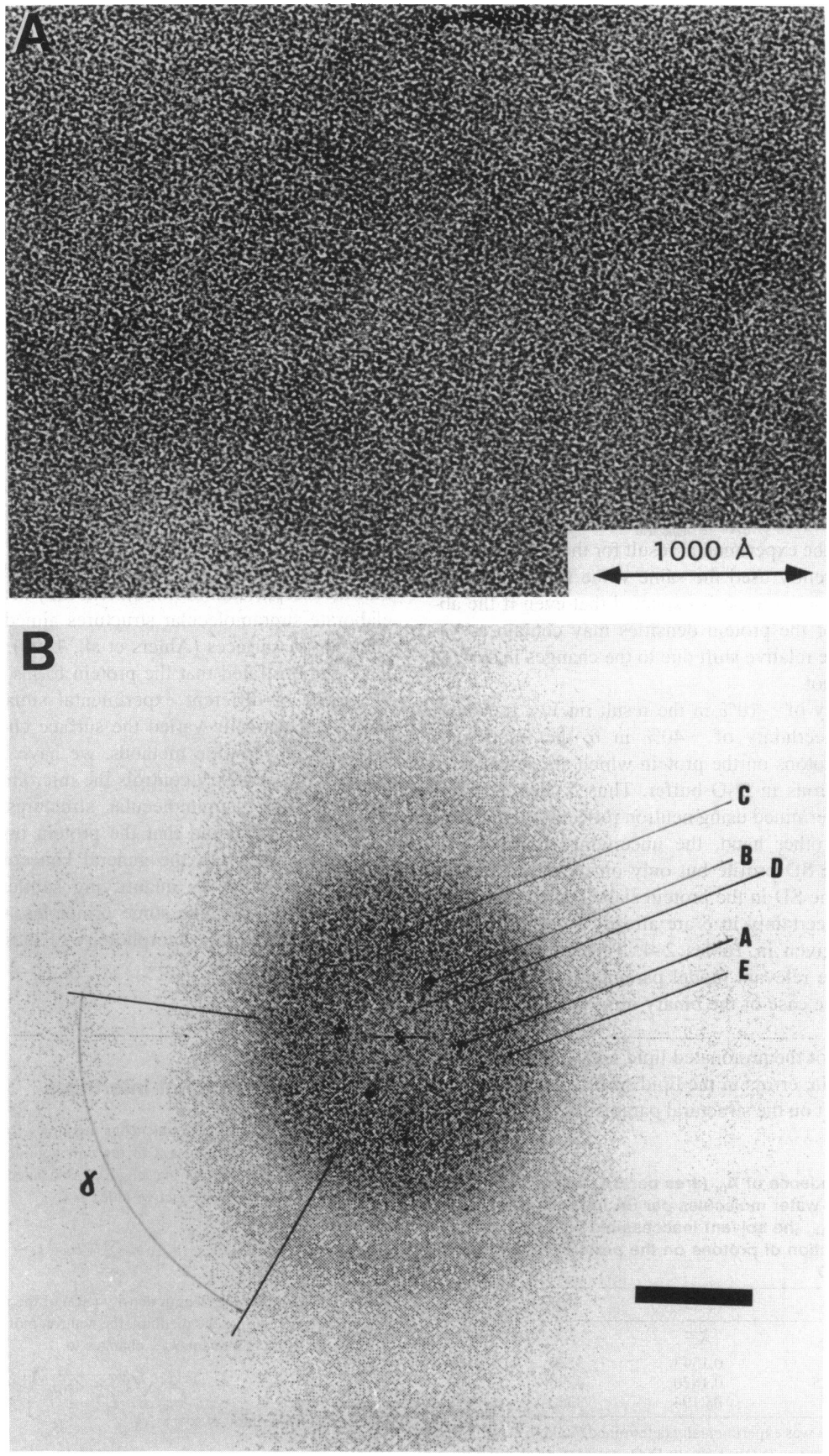

FIGURE 12 (*a*) High-magnification electron micrograph of the sample shown in Fig. 11. The scale bar is 1000 Å. (*b*) Fourier transform of a digitized image from a square (166 × 166 nm^2) section of *a*. Five Fourier peaks are indicated. The scale bar is $(25\ Å)^{-1}$.

refinements based on individual data sets (see footnote in Results). We conclude therefore that both protein phases are comparable in their average density, and stress that the reported structural properties are not the properties of the domain phase, but constitute an average over macroscopic areas.

A correct determination of the solvent inaccessible volume of the protein, V_{SA}, is indispensable for a correct assessment of proton exchange on the protein in D_2O buffer, and thus of protein's surface density. V_{SA} = 66,000 ± 6,000 Å^3 has been determined from combined x-ray and neutron reflectivity measurements (Vaknin et al., 1993). This result translates into a SD of the dry perprotonated protein of $\rho_{SA} = 2.08 \times 10^{-6}$ Å^{-2} and agrees well with typical results from neutron scattering on protein solutions (Perkins, 1988). From the amino acid composition of the SA tetramer (Green, 1975) and in conjunction with the volumes occupied by amino acid monomers in single crystals (see Perkins (1988), p. 155) one can compute a composite volume which is also close to the determined value for V_{SA}: $\Sigma^{SA}_{\text{amino acid}}$ = 69,370 Å^3 agrees again well with the experimental result for the protein. Since we have consistently used the same value for V_{SA} for the modeling of all data sets, it is expected that even if the absolute results for the protein densities may contain a systematic error, the relative shift due to the changes in surface chemistry will not.

An uncertainty of ~10% in the result on V_{SA} translates into a large uncertainty of ~40% in δ, the fraction of exchangeable protons on the protein which are actually replaced by deuterons in D_2O buffer. Thus δ cannot be experimentally determined using neutron reflectivity measurements. On the other hand, the uncertainty in δ has no influence on the SD profile but only on the molecular interpretation of the SD in the protein slab. The errors resulting from the uncertainty in δ are already accounted for in the error bars given in Tables 2–4. Table 5 displays the sensitivity of the relevant model parameters to changes in δ and V_{SA} for the case of the binary mixture of DMPC and B-cap-DPPE.

Since the SD of the protonated lipid is much smaller than that of the protein, errors in the lipid surface density have a negligible impact on the structural parameters deduced from neutron data for the protein aggregates. In the single case where the neutron reflectivity measurements are sensitive to the lipid chains, i.e., for binary mixtures employing DMPC-d_{54}, we have detected a significant decrease of the surface density of lipids after the application of the protein to the subphase, most probably due to destruction inferred in the surface monolayer by multiple perforation with the syringe. We have not accounted for such a rearrangement in the cases of pure B-cap-DPPE and of binary mixtures with cholesterol since we had no means of determining precisely the structural changes. The general conclusions on the structure are not affected by this omission.

TABLE 5 Dependence of A_{pr} (area per SA molecule) and of n_w^{pr} (number of water molecules per SA in the hydrated monolayer) on V_{SA}, the solvent inaccessible volume, and on δ, the fraction of protons on the protein, which exchanges in D_2O

V_{SA}	δ	SD(SA,D_2O)	A_{pr}	n_w^{pr}
Å^3	%	Å^{-2}	Å^2	
60,000	20	0.1543	3230	2310
66,000	57.5	0.1870	3295	2180
72,000	95	0.2194	3350	2070

V_{SA} = 66,000 ± 10% was experimentally determined (Vaknin et al., 1993). Scattering length densities (SD) of SA in D_2O, calculated for different δ, are also given. The four data sets for DMPC/B-cap-DPPE (3:1) at π = 15 mN/m, $T \sim 18$°C, were simultaneously evaluated. Note that V_{SA} and δ are strongly coupled, i.e., χ^2 is identical for all parameter sets shown.

CONCLUSIONS

In previous work it has been shown that SA forms well defined molecular layers upon adsorption from dilute solutions to biotin-functionalized interfaces (Darst et al., 1991; Vaknin et al., 1991a; Lösche et al., 1992; Lösche, 1992; Vaknin et al., 1993; Blankenburg et al., 1989; Herron et al., 1992; Schmidt et al., 1992). It was thus proposed that the streptavidin-biotin system may serve as a basis for elaborate supramolecular structures aimed at the functionalization of surfaces (Ahlers et al., 1990). In this work we have demonstrated that the protein forms surface layers in a number of different experimental situations, where we have systematically varied the surface chemistry, and, using contrast variation methods, we have investigated how the surface chemistry controls the micromorphology of the self-assembled supramolecular structures. In all investigated cases we found that the protein organizes in structures consistent with the general conception used in our earlier work, and, by quantifying subtle differences, we were able to formulate some principles, which we postulate might control the morphology of these self-assembled systems.

APPENDIX

Neutron reflectivity of interfaces

The refractive index of a homogeneous medium i for neutrons, n_i, can be *calculated* if the atomic content of the unit volume, V_i, is known. Each atomic species j has a scattering length b_j associated with it. If ν_j atoms j are located within V_i the refractive index is

$$n_i = 1 - \frac{\lambda^2}{2\pi} \times \frac{1}{V_i} \times \sum_{j \text{ in } V_i} \nu_j b_j = 1 - \frac{\lambda^2}{2\pi} \rho_i, \qquad \text{(A1)}$$

where ρ_i is the scattering length density (SD) of the medium i. Upon traveling from vacuum into the medium, the neutron momentum changes from $\vec{k}_o$ to $\vec{k}_i$ and its z component, $k_{o,z}$, changes to

$$k_{i,z} = \sqrt{k_{o,z}^2 - 4\pi\rho_i}. \qquad \text{(A2)}$$

This can be re-written as

$$k_{i,z} = \sqrt{k_{o,z}^2 - k_{i,c}^2}, \qquad \text{(A3)}$$

where $k_{i,c}$ is the critical value of k_z for total reflection. The reflectivity from an ideal interface between two media, where the SD changes

discontinuously, is

$$R_{i,i+1} = r_{i,i+1} r^*_{i,i+1} \tag{A4a}$$

with

$$r_{i,i+1} = \frac{k_{i,z} - k_{i+1,z}}{k_{i,z} + k_{i+1,z}}. \tag{A4b}$$

r represents the *reflection amplitudes* and the asterisk denotes the complex conjugate. If there is only one interface, separating a (semi-infinite) substrate, 1, from a vacuum compartment, the resulting reflectivity is the *Fresnel* reflectivity,

$$R_F = R_F(k_{o,z}) = \left| \frac{1 - \sqrt{1 - (k_{1,c}/k_{o,z})^2}}{1 + \sqrt{1 - (k_{1,c}/k_{o,z})^2}} \right|^2 \tag{A5}$$

which can be approximated at $k_{o,z2} \gg k_{1,c}{}^2$ as

$$R_F \sim \left(\frac{k_{1,c}}{k_{o,z}}\right)^4 \sim \left(\frac{Q_c}{Q_z}\right)^4. \tag{A6}$$

The reflectivity decreases with the fourth power of $k_{o,z}$ (or of $Q_z = 2k_{o,z}$, as reflectivity curves are usually presented as a function of the momentum transfer).

For the case of a stratified sample with sharp interfaces, multiple reflections occur at each interface, giving rise to interference between the different reflected beams. If only one layer of thickness d_1 is located between semi-infinite vacuum and subphase compartments, 0 and 2, the reflection amplitude at this slightly more complicated surface is

$$r = \frac{r_{0,1} + r_{1,2} \exp(2ik_{1,z}d_1)}{1 + r_{0,1}r_{1,2} \exp(2ik_{1,z}d_1)}. \tag{A7}$$

As before, the reflectivity is computed by multiplication with the complex conjugate of r and contains oscillatory functions of Q_z (via $k_{1,z}$ which depends on $k_{o,z}$), that are formally due to the exponential arguments in Eq. A7 and comprise the fingerprint of the interference effects. The amplitude of these oscillations, for example, is related to the contrast between the different media, as seen from the fact that the $r_{i,i+1}$ determine the magnitude of the exponentials at constant k and d. Multiple layered systems may be analyzed by using a recursion formula based on the reflectivity of the one-layer system and by working up from the bottom layer to the top. It is easy to see that the solutions are not straightforward or intuitive, nor can they be given in general as a closed analytic solution. They can in principle be obtained, however, from numerical computations (Parratt, 1954), and, provided the thickness values d_i are chosen small enough, any arbitrary profile of the SD at the interface can be approximated by such a multilayer structure.

For a real liquid interface, surface roughness has to be taken into account. It can be thought of as being introduced by thermally excited capillary waves with amplitudes in the Ångstrom regime and may be modeled as a Gaussian smearing of the sharp step in refractive index between interfaces (Als-Nielsen and Kjaer, 1989). The impact of interface roughness is to decrease the reflectivity of a surface at high Q_z to below the values expected from the Q_z^{-4} law.[2] (Analogously, due to an increase in diffuse scattering, a frozen glass pane offers less specular light reflection than a clear pane does at progressively larger incidence angles.) The rough surface scatters some radiation into nonspecular directions and this may appear as an elongated tail to the specularly reflected beam, i.e., for these contributions is $Q_x \neq 0$ and $Q_y \neq 0$. The geometry of detuning the specular reflection condition for the experimental characterization of the surface roughness (Sinha et al., 1988) is depicted for the Q_y component in Fig. A1, where an angle $\Delta\alpha_r = 2\varphi$ is scanned to observe the decay of the signal, and for the Q_x component in Fig. A2, where an equivalent horizontal scattering angle, 2θ, is scanned.

A perfectly equivalent approach to the calculation of the reflectivity of an interface, which gives more physical insight into the relationship between

[2] Due to the gradual change in density, the transmission of the interface is also augmented.

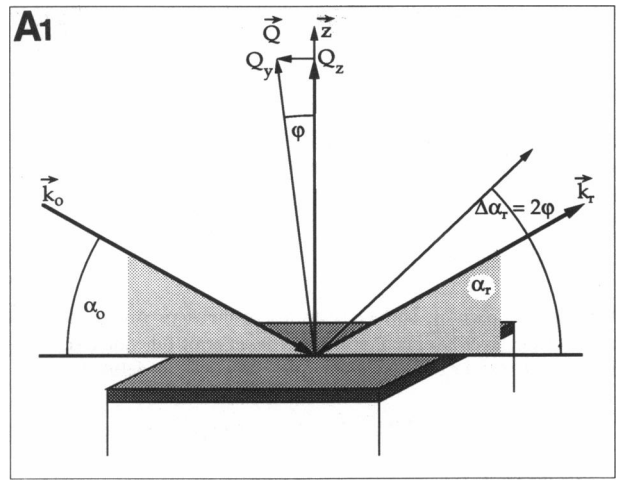

FIGURE A1 A scan of the nonspecular reflection angle, α_r, around α_o leads to a momentum transfer with a horizontal component $Q_y > 0$.

the SD profile and the final result, is the kinematical approximation (Als-Nielsen et al., 1982; Braslau et al., 1988). It relates the Fresnel normalized reflectivity, R/R_F, to the Fourier transform of the *spatial changes* of the SD profile parallel to $\vec{z}$ and to the SD of the substrate, ρ_{bulk}:

$$\frac{R(Q_z)}{R_F(Q_z)} = \frac{1}{\rho^2_{bulk}} \left| \int_{interface} \frac{d\rho(z)}{dz} \exp(iQ_z z) dz \right|^2. \tag{A8}$$

In this simplest form, the kinematical representation uses an approximation for the phases in the argument of the exponential. Including a refraction correction, i.e., using a more sophisticated description of the phases, it can be demonstrated for molecularly thin layers with low absorption that

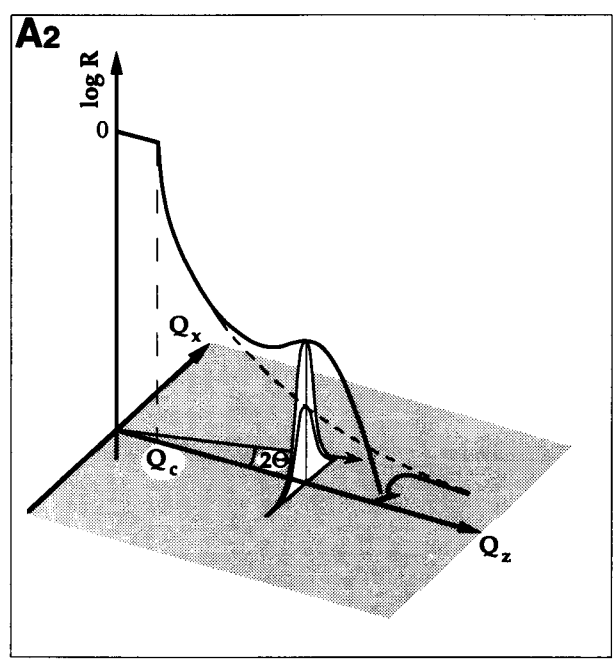

FIGURE A2 Scanning the horizontal diffraction angle, 2θ, leads to nonzero values of the horizontal momentum transfer component Q_x. A schematic presentation of reflectivity curves, log R vs. Q_z, is also included. Dashed line: Fresnel reflectivity, R_F, of the substrate; solid line: hypothetical reflectivity signal, R, of a stratified interface. Below the critical angle for total reflection, Q_c, the observed value of R is unity.

both computation techniques lead to identical results for all except very small momentum transfer values, $Q_z \sim Q_c$, where multiple scattering effects have been neglected in the kinematical approach (Als-Nielsen and Kjaer, 1989).

If $(d\rho(z)/dz)$ is modeled by a simple one-box approximation with surface roughness σ, i.e., when the surface is conceived as covered with one homogeneous layer of thickness d and SD ρ_l, Eq. A8 can be expressed as

$$\frac{R(Q_z)}{R_F(Q_z)} = \frac{1}{\rho_{bulk}^2}\left|\left\{(\rho_{bulk} - \rho_l) + \rho_l \exp(-iQ_z d)\right\}\exp\left(-\frac{1}{2}Q_z^2\sigma^2\right)\right|^2 \quad \text{(A9)}$$

where in real space the surface smearing of the steps $\Delta\rho_i$ at the top and bottom of the layer has been modeled with an error function (Als-Nielsen and Kjaer, 1989), i.e., around $z = 0$, the SD profile is defined as:

$$\rho(z) = \frac{\rho_{bulk} - \rho_l}{2} \times [1 - \mathrm{erf}(z/\sqrt{2\sigma})]. \quad \text{(A10)}$$

For small angles where the surface roughness may be neglected, $Q_z\sigma \ll 1$, this reduces to

$$\frac{R(Q_z)}{R_F(Q_z)} = \frac{1}{\rho_{bulk}^2} \times [(\rho_{bulk} - \rho_l)^2 + \rho_l^2 + 2\rho_l(\rho_{bulk} - \rho_l)\cos(Q_z d)], \quad \text{(A11)}$$

which may be used to semiquantitatively estimate the overall thickness of an interface structure, since the minimum in reflectivity is at $Q_z d = \pi$ if $\rho_l < \rho_{bulk}$.

We thank J. Als-Nielsen, H. Möhwald, H. Ringsdorf, and M. Seul for helpful discussions. D. Vaknin, M. Lösche, and M. Piepenstock are gratefully indebted to colleagues at Risø National Laboratory for their hospitality and many useful discussions. M. Lösche and A. Diederich wish to acknowledge the invaluable guidance of A. Brisson in the preparation of EM samples, the assistance of P. Simon with the EM work, and the opportunity to use the EM facilities in the group of I. M. Voigt-Martin.

The work at Risø was supported by the NOVO and Carlsberg foundations and by the Danish Natural Science Research Council. Financial support from the German Bundesministerium für Forschung und Technologie under contract 05 453 FA I9 and from the Deutsche Forschungsgemeinschaft under contract Lo352/3 is gratefully acknowledged. Ames Laboratory is operated under the U. S. Department of Energy by Iowa State University under contract W-7405-Eng-82. This work was supported by the Director for Energy Research, Office of Basic Energy Sciences.

REFERENCES

Adamson, A. W. 1990. Physical Chemistry of Surfaces, 5th edition, chapter IX. John Wiley, New York.

Ahlers, M., W. Müller, A. Reichert, H. Ringsdorf, and J. Venzmer. 1990. Specific interactions of proteins with functional lipid monolayers—ways of simulating biomembrane processes. *Angew. Chem. Int. Ed. Engl.* 29: 1269–1285.

Alberts, B., D. Bray, J. Lewis, M. Raff, and J. D. Watson. 1983. Molecular Biology of the Cell. Garland, New York.

Albrecht, O., H. Gruler, and E. Sackmann. 1978. Polymorphism of phospholipid monolayers. *J. Phys. (Paris).* 39:301–313.

Als-Nielsen, J., F. Christensen, and P. S. Pershan. 1982. Smectic-A order at the surface of a nematic liquid crystal: synchrotron x-ray diffraction. *Phys. Rev. Lett.* 48:1107–1110.

Als-Nielsen, J., and K. Kjaer. 1989. X-ray reflectivity and diffraction studies of liquid surfaces and surfactant monolayers. *In* Phase Transitions in Soft Condensed Matter. T. Riste and D. Sherrington, editors. Plenum Press, New York. 113–138.

Bibo, A. M., C. M. Knobler, and I. R. Peterson. 1991. A monolayer phase miscibility comparison of long-chain fatty acids and their ethyl esters. *J. Phys. Chem.* 95:5591–5599.

Blankenburg, R., P. Meller, H. Ringsdorf, and C. Salesse. 1989. Interaction between biotin lipids and streptavidin monolayers: formation of oriented two-dimensional protein domains induced by surface recognition. *Biochemistry.* 28:8214–8221.

Braslau, A., P. S. Pershan, G. Swislow, B. M. Ocko, and J. Als-Nielsen. 1988. Capillary waves on the surface of simple liquids measured by x-ray reflectivity. *Phys. Rev. A.* 38:2457–2470.

Cadenhead, D. A., F. Müller-Landau, and B. M. J. Kellner. 1980. Phase transitions in insoluble one and two-component films at the air/water interface. *In* Ordering in Two Dimensions. S. K. Sinha, editor. Elsevier/North Holland, Amsterdam. 73–81.

Carr, P. W., and L. D. Bowers. 1980. Immobilized Enzymes in Analytical Applications and Clinical Chemistry. John Wiley, New York.

Chaiet, L., and F. J. Wolf. 1964. The properties of streptavidin, a biotin-binding protein produced by streptomycetes. *Arch. Biochem. Biophys.* 106:1–5.

Darst, S. A., M. Ahlers, P. H. Meller, E. W. Kubalek, R. Blankenburg, H. O. Ribi, H. Ringsdorf, and R. D. Kornberg. 1991. Two-dimensional crystals of streptavidin on biotinylated lipid layers and their interaction with biotinylated macromolecules. *Biophys. J.* 59:387–396.

Ebersole, R. C., J. A. Miller, J. R. Moran, and M. D. Ward. 1990. Spontaneously formed functionally active avidin monolayers on metal surfaces: a strategy for immobilizing biological reagents and design of piezoelectric biosensors. *J. Am. Chem. Soc.* 112:3239–3241.

Egger, M., S. Heyn, and H. E. Gaub. 1990. Two-dimensional recognition pattern of lipid-anchored fab' fragments. *Biophys. J.* 57:669–673.

Green, N. M. 1975. Avidin. *In* Advances in Protein Chemistry. M. L. Anson and J. T. Edsell, editors. Academic Press, New York. 85–133.

Gronow, M. 1991. Biosensors—"A marriage of biochemistry and microelectronics." *In* Biotechnology—the Science and the Business. V. Moses and R. E. Cape, editors. Harwood Academic, London. 355–370.

Haas, H., and H. Möhwald. 1993. Pressure dependent arrangement of a protein in two-dimensional crystals specifically bound to a monolayer. *Colloids Surf. B: Biointerfaces.* 1:139–148.

Hafeman, D. G., V. V. Tscharner, and H. M. McConnell. 1981. Specific antibody-dependent interactions between macrophages and lipid haptens in planar lipid monolayers. *Proc. Natl. Acad. Sci. USA.* 78:4552–4556.

Henderson, R., J. M. Baldwin, T. A. Ceska, F. Zemlin, E. Beckmann, and K. H. Downing. 1990. Model for the structure of bacteriorhodopsin based on high-resolution electron cryomicroscopy. *J. Mol. Biol.* 213:899–929.

Hendrickson, W. A., A. Pähler, J. L. Smith, Y. Satow, E. A. Merritt, and R. P. Phizackerley. 1989. Crystal structure of core streptavidin determined from multiwavelength anomalous diffraction of synchrotron radiation. *Proc. Natl. Acad. Sci. USA.* 86:2190–2194.

Herron, J. N., W. Müller, M. Paudler, H. Riegler, H. Ringsdorf, and P. A. Suci. 1992. Specific recognition-induced self-assembly of a biotin lipid/streptavidin/Fab fragment triple layer at the air/water interface: ellipsometric and fluorescence microscopy investigations. *Langmuir.* 8: 1413–1416.

Lösche, M. 1992. Structural characterization of molecular interface layers using neutron and x-ray reflectivity techniques. *In* Synthetic Microstructures in Biological Research. J. M. Schnur and M. Peckarar, editors. Plenum Press, New York. 91–108.

Lösche, M., and H. Möhwald. 1984. Fluorescence microscope to observe dynamical processes in monomolecular layers at the air/water interface. *Rev. Sci. Instrum.* 55:1968–1972.

Lösche, M., M. Piepenstock, D. Vaknin, and J. Als-Nielsen. 1992. Molecular recognition processes at functionalized lipid surfaces: a neutron reflectivity study. *Thin Solid Films.* 210/211:659–661.

Ludwig, S. D., H. O. Ribi, G. K. Schoolnik, and R. D. Kornberg. 1986. Two-dimensional crystals of cholera toxin B subunit-receptor complexes: projected structure at 17-Å resolution. *Proc. Natl. Acad. Sci. USA.* 83: 8585–8588.

Möhwald, H. 1990. Phospholipid and phospholipid-protein monolayers at the air/water interface. *Annu. Rev. Phys. Chem.* 41:441–476.

Mosser, G., and A. Brisson. 1991. Conditions of two-dimensional crystallization of cholera toxin B-subunit on lipid films containing ganglioside GM1. *J. Struct. Biol.* 106:191–198.

Mosser, G., C. Ravanat, J.-M. Freyssinet, and A. Brisson. 1991. Sub-domain structure of lipid-bound annexin-V resolved by electron image analysis. *J. Mol. Biol.* 217:241–245.

Nagle, J. F., and M. C. Wiener. 1988. Structure of fully hydrated bilayer dispersions. *Biochim. Biophys. Acta.* 942:1–10.

Nargessi, R. D., and D. S. Smith. 1986. Fluorometric assays for avidin and biotin. *Methods Enzymol.* 122:67–73.

Parratt, L. G. 1954. Surface studies of solids by total reflection of x-rays. *Phys. Rev.* 95:359–369.

Perkins, S. J. 1988. X-ray and neutron solution scattering. *In* Modern Physical Methods in Biochemistry, Part B, Chapter 6. A. Neuberger and L. L. M. V. Deenen, editors. Elsevier/North Holland, Amsterdam. 143–265.

Pisarchick, M. L., and N. L. Thompson. 1990. Binding of a monoclonal antibody and its Fab fragment to supported phospholipid monolayers measured by total internal reflection fluorescence microscopy. *Biophys. J.* 58:1235–1249.

Reed, R. A., J. Mattai, and G. G. Shipley. 1987. Interaction of cholera toxin with ganglioside G_{M1} receptors in supported lipid monolayers. *Biochemistry.* 26:824–832.

Ribi, H. O., P. Reichard, and R. D. Kornberg. 1987. Two-dimensional crystals of enzyme-effector complexes: ribonucleotide reductase at 18-Å resolution. *Biochemistry.* 26:7974–7979.

Russell, T. P. 1990. X-ray and neutron reflectivity for the investigation of polymers. *Mater. Sci. Rep.* 5:171–271.

Sagiv, J. 1980. Organized monolayers by adsorption. I. Formation and structure of oleophobic mixed monolayers on solid surfaces. *J. Am. Chem. Soc.* 102:92–98.

Sanyal, M. K., S. K. Sinha, K. G. Huang, and B. M. Ocko. 1991. X-ray-scattering study of capillary-wave fluctuations at a liquid surface. *Phys. Rev. Lett.* 66:628–631.

Schmidt, A., J. Spinke, T. Bayerl, E. Sackmann, and W. Knoll. 1992. Streptavidin binding to biotinylated lipid layers on solid support. *Biophys. J.* 63:1185–1192.

Sinha, S. K., E. B. Sirota, S. Garoff, and H. B. Stanley. 1988. X-ray and neutron scattering from rough surfaces. *Phys. Rev. B.* 38:2295–2311.

Swalen, J. D., J. Allara, J. D. Andrade, E. A. Chandross, S. Garoff, J. Israelachvili, T. J. McCarthy, R. Murray, R. F. Pease, J. F. Rabolt, K. J. Wynne, and H. Yu. 1987. Molecular monolayers and films. *Langmuir.* 3:932–950.

Tamm, L. K. 1988. Lateral diffusion and fluorescence microscope studies on a monoclonal antibody specifically bound to supported phospholipid bilayers. *Biochemistry.* 27:1450–1457.

Tidswell, I. M., B. M. Ocko, P. S. Pershan, S. R. Wasserman, G. M. Whitesides, and J. D. Axe. 1990. X-ray specular reflection studies of silicon coated by organic monolayers (alkylsiloxanes). *Phys. Rev. B.* 41: 1111–1128.

Uzgiris, E. E., and R. D. Kornberg. 1983. Two-dimensional crystallization technique for imaging macromolecules, with an application to antigen-antibody-complement complexes. *Nature (Lond.).* 301:125–129.

Vaknin, D., J. Als-Nielsen, M. Piepenstock, and M. Lösche. 1991a. Recognition processes at a functionalized lipid surface observed with molecular resolution. *Biophys. J.* 60:1545–1552.

Vaknin, D., K. Kjaer, J. Als-Nielsen, and M. Lösche. 1991b. A new liquid surface neutron reflectometer and its application to the study of DPPC in a monolayer at the air/water interface. *Makromol. Chem. Macromol. Symp.* 46:383–388.

Vaknin, D., K. Kjaer, J. Als-Nielsen, and M. Lösche. 1991c. Structural properties of phosphatidylcholine in a monolayer at the air/water interface. Neutron reflection study and reexamination of x-ray reflection experiments. *Biophys. J.* 59:1325–1332.

Vaknin, D., K. Kjaer, H. Ringsdorf, R. Blankenburg, M. Piepenstock, A. Diederich, and M. Lösche. 1993. X-ray and neutron reflectivity studies of a protein monolayer adsorbed to a functionalized aqueous surface. *Langmuir.* 9:1171–1174.

Weber, P. C., D. H. Ohlendorf, J. J. Wendolowski, and F. R. Salemme. 1989. Structural origins of high-affinity biotin binding to streptavidin. *Science (Wash. DC).* 243:85–88.

Wiener, M. C., and S. H. White. 1991. Fluid bilayer structure determination by the combined use of x-ray and neutron diffraction II. "Composition-space" refinement method. *Biophys. J.* 59:174–185.

Wiener, M. C., and S. H. White. 1992. Structure of a fluid dioleoylphosphatidylcholine bilayer determined by joint refinement of x-ray and neutron diffraction data. III. Complete structure. *Biophys. J.* 61:434–447.

Wilchek, M., and E. A. Bayer. 1988. The avidin-biotin complex in bioanalytical applications. *Anal. Biochem.* 171:1–32.

Zhou, X.-L., and S.-H. Chen. 1993. Model-independent method for reconstruction of scattering-length-density profiles using neutron and x-ray reflectivity data. *Phys. Rev. E.* 47:3174–3190.